CHARACTERIZATION OF SANDS FOR HEAVY MINERALS, SELECTED HEAVY METALS DISTRIBUTION AND PROFILING ALONG RIVER TIVA, KITUI COUNTY, SOUTHEASTERN KENYA

By

Kiprotich Kilel Kennedy, BSc (Analytical Chemistry)

A thesis submitted for examination in partial fulfillment of the requirements for the award of the degree of Master of Science in Nuclear Science, University of Nairobi

DECLARATION

I declare that this thesis is my original work and has not been presented to any other University for the purposes of an award of any degree programme.

S56/74421/2012

Kiprotich Kilel Kennedy

Institute of Nuclear Science and Technology, University of Nairobi

Signature…….Date…….

This thesis has been submitted for examination by our approval as University supervisors:

1) Mr. Michael. J. Mangala
   Institute of Nuclear Science and Technology, University of Nairobi
   Signature……..Date……

2) Prof. Eliud .M. Mathu
   Institute of Mining and Mineral Processing, South Eastern University Kenya (SEKU)
   Signature……..Date...……

3) Mr. David .M. Maina
   Institute of Nuclear Science and Technology, University of Nairobi
   Signature…….Date……...

DEDICATION

I dedicate this thesis to my son Seth Bragg Cheruiyot, my wife Naomi and my mother, Rael.

ABSTRACT

The main objective of this study was to characterize the river Tiva sands for heavy mineral content. The study, in addition, has determined the elements associated with heavy minerals of interest; titanium (Ti), iron (Fe) and zirconium (Zr) in 47 samples that were randomly sampled from 10 site locations representing Kalimbevo, Nduumoni and Tanganyika at the surface and at the depth of 0.3 -0.5m. Sampling was done along river Tiva for a stretch of 3 Km along the river course between 3rd and 5th June, 2012.

The sand samples were dried to constant weight, pulverized, sieved and pelletized before analysis by Energy Dispersive X-ray fluorescence (EDXRF). The sand samples were prepared in aliquots of triplicate pellets of a diameter of 2.5cm and weighed between 0.3-0.5g. The elemental determination was done using an Energy Dispersive X-ray Fluorescence spectrometer (EDXRF), Shimadzu (EDX 800HS) available at the Department of Materials and Testing Laboratories in the Ministry of Infrastructure and Transport. Each sample pellet was irradiated for the 50s. X-ray diffraction (XRD) analyses were done at ICRAF using Bruker, D2 Phaser spectrometer for mineral identification. Principal component analysis (PCA) was performed on the results of elemental concentrations to determine the correlation between the elements and the source of the heavy minerals.

In general, this study found out that the mean values of; iron (Fe) to be 73135±6027µg/g, titanium (Ti) 22976±1971µg/g and zirconium (Zr) 1115±136µg/g. XRD results of analyses showed the existence of ilmenite and hematite as some of the heavy minerals present in these samples. Element Fe/Ti ratios were used to determine titanomagnetite properties, in addition to regression and principal component analysis (PCA) in determining the source of the elements.

Results of EDXRF data obtained showed iron oxide (Fe_2O_3) to average 10.46%; titanium dioxide (TiO_2) results average at 3.83% and that approximately 80% of the iron in these samples is confined to magnetite and a proportionate relationship between iron and titanium dioxide is indicative of significant titanomagnetite content described by PCA analysis of the results.

The distribution of these elements was studied along the river, across, and at depths along the river Tiva profile. The results show that elemental concentration increases downstream except at convex of the river where there are elevated concentrations. In general, high elemental concentration was also found in the subsurface samples of the river bed than at the depth of the riverbed at 50cm. For example, the average Fe concentration at the subsurface is 104328µg/g compared to 51016µg/g at the depth of 50cm; a similar trend is replicated for Ti (34033µg/g against 14635µg/g) and zirconium (Zr) was found to be in low concentration (1529µg/g against 593µg/g). There is no statistical significant difference in the elemental concentration distribution across the river bed, following the ANOVA analyses.

In conclusion, this study has demonstrated the potential existence of titanium bearing heavy minerals in river Tiva sands and recommends; Heavy mineral separation studies, Provenance studies, complementary characterization techniques for heavy minerals, interrelationship between river Tiva and Kwale heavy mineral sands and ilmenite alteration studies.

ACKNOWLEDGEMENT

I would like to extend my profound appreciation to Mr. Michael J. Mangala and Mr. David M. Maina Lecturers, Institute of Nuclear Science and Technology, UoN. Also, to Professor Eliud M. Mathu of the Institute of Mining and Mineral Processing, South Eastern Kenya University (SEKU) for their valuable professional guidance and constructive suggestions in the preparation of this thesis and facilitation of research resources.

I would also like to thank Mr.Simon Bartilol, the Chief Technologist, Institute of Nuclear Science and Technology, University of Nairobi (UoN) for his assistance in sample preparations and analyses; the Chief Chemist, Mr. Namu and Mrs. Faith, Chemistry Section, Materials and Testing Research Laboratories, Ministry of Infrastructure and Transport for allowing me to use their Shidmazu EDXRF-800HS spectrometer and pulverizer, for sample preparation and EDXRF analyses, and the staff of ICRAF for XRD analyses of few selected samples for mineral analyses.

My special thanks go to the CEO, Hon Ochillo Ayako, and Kenya Nuclear Electricity Board (KNEB) for awarding me the scholarship to pursue Master's degree program at the Institute of Nuclear Science and Technology, University of Nairobi and the National Council of Science Technology and Innovation (NACOSTI) for financing the field work for this thesis research project.

Lastly, I thank the Almighty God for divine help, energy, and wisdom, throughout the study period.

TABLE OF CONTENTS

Page No

LIST OF FIGURES

LIST OF TABLES

APPENDICES

ACRONYMS AND ABBREVIATIONS

ANOVA	Analysis of Variance
EDXRF	Energy Dispersive X-Ray Fluorescence
GDP	Gross Domestic Product
GPS	Geographical Positioning System
HMS	Heavy Mineral Sand
ICRAF	International Centre for Research in Agroforestry
IPA	Isopropyl Alcohol
LLD	Lower Limit of Detection
LOD	Limit of Detection
NACOSTI	National Council of Science Technology and Innovation
PCA	Principal Component Analysis
WDXRF	Wavelength Dispersive X-ray Fluorescence
XRD	X-Ray Diffractometer
XRF	X-Ray Fluorescence

CHAPTER ONE

INTRODUCTION

1.1 Background Information

Kenya aims to increase its annual GDP growth rate to 10% and to become a choice for the provision of basic manufactured goods in Eastern and Central Africa in its long-term development plans (Vision 2030, 2007). This will be achieved by investing in areas amongst others, which include mineral exploitation, thereby providing raw materials necessary for the manufacturing sector.

To date, the mining industry in Kenya is perceived to account for an insignificant proportion of the GDP, largely due to lack of developed infrastructure and appropriate policies to spur production (Munyiri, 2009). However, a wide variety of minerals both ore and non-ore is undiscovered (Rop, 2010). In general, minerals found in Kenya include; soda ash, fluorspar, barite, gypsum, salt, nickel, graphite, kaolin, copper, rare earth elements and heavy minerals (Mesfin et al., 2006).

Heavy minerals such as ilmenite, rutile, zircon, and garnet are important economic resources and are useful in many industrial applications including; used as raw materials for nuclear power production industry, and also in the manufacture of metallurgical and engineering industrial products (Grosz and Schruben,1994).

Economic heavy minerals in the coastal zone in general have attracted much interest in exploration and exploitation in various places worldwide (Gent et al., 2005). In Kenya, deposits of heavy minerals are located in Kwale, Coast of Kenya where titanium mining is undertaken by Base Titanium Kenya Limited.

Previously, it has been proposed that there are precious mineral ores in the rocks underlying the Mozambique belt, which runs from the north through central to the coastal part of Kenya (Kariuki, 2002). Based on results of these studies, Base Resources Ltd of Australia in 2010 acquired the Kwale mineral sands deposits with the aim of mineral exploitation of titanium and zirconium (Base Resources, 2011). In general, Kwale is

characterized by sedimentary rocks which are the possible sources of heavy mineral sands mineralization (Kariuki, 2002).

According to Tyler and Minnitt (2004), surficial dune and paleo-dune deposits of chemically inert and physically resistant heavy mineral sands (HMS) occur along the sub-Saharan coastline. Worldwide these are the sources of titanium, titanium dioxide, and zircon. About 75% of the world's titanium production is from heavy mineral sands, the rest being extracted mainly from hard rock (TZMI, 2001). HMS deposits contain proportions of heavy minerals that vary from 10 wt% to 35 wt% with economies of the scale being advantageous for larger deposits (Rozendaal et al., 1999). Rutile and ilmenite are the most important sources of titanium dioxide (TiO_2) and are indirect sources of titanium metal. High demand for iron samples in the recent years, particularly in China, has led to the exploitation of the lower grade iron deposits (30%-64%) worldwide and expanded to include other banded iron formation typical of 20-40% Fe (Volp et al., 2009), and in the production of iron ore from heavy mineral sands tailings at Iluka projects in Australia (Volp et al., 2009).

The Kitui region is located within the Proterozoic Mozambique Belt, which is most extensive in Central Kenya and extends from north to south; has minerals associated with granitic rocks (Kariuki, 2002). The region is characterized by sedimentary rocks of Paleozoic to Quaternary, which are major sources of heavy mineral sands (Kariuki, 2002). These characteristics offer the possibility for the existence of heavy mineral sands and other minerals.

This study has, therefore, provided additional data for the existence of elements associated with heavy mineral sands and for their characterization, specifically iron, titanium, and zirconium.

Worldwide, it is recognized that various similar studies, for example in India of a two stage model for pseudo-rutile formation from Ilmenites of Manavalakurichi region has been reported (Subramanyam et al., 1982) and the alteration of ilmenite from river Valliyar detailed (Nair et al., 1995). Along the Ratnagiri coast, the provenance of the

offshore ilmenite based on geochemical studies has been undertaken (Rajamanickam et al., 1997).

Chandrajith (2001) investigated the stream sediments geochemistry of the Walawe Ganga Basin of the Sri Lanka and found high enrichment for some of the trace elements; Zr, Ti, Hf and Nb, an indication of the existence of mineralized terrains within the fields.

Abuodha (2003) determined grain size distribution and heavy mineral content of beach and dune sediments from Malindi Bay coast. He determined grain size by dry sieving sediments and found that heavy minerals vary from 15% to 67% by weight. However, there are limited studies detailing the existence of the heavy minerals in the river sediments in Kenya, in general.

In practice, geochemical prospecting for minerals involves systematic measurement of one or more chemical occurring material for purposes of determining the chemical pattern indicative of the presence of the ore in the vicinity (Hawkes, 1957), most often, achieved by averaging abundance of the certain elements and determining the formation of geochemical anomalies (Pourjabbar and Hezarkhani,2006). A thorough understanding of geochemical anomalies is fundamental for effective geochemical prospecting (Pourjabbar and Hezarkhani, 2006).

This study sought to determine; the heavy mineral content, their distribution, profiling and characterization of river Tiva sediment samples in Kitui County using X-ray fluorescence and X-ray diffraction (XRD).

1.2 Description of the Study Area

1.2.1 Geographical and Topographical Description

The study area is located in Kitui County, 160 Km south-east of the city of Nairobi specifically Kwa-Vonza location, at an elevation between 482m to 2053m above the sea level.

River Tiva has two tributaries; the Mikuyuni and Mwita-Syano Rivers, and eventually drains into Tana River. The sampling area along river Tiva is bound by WGS 1984 coordinate (-1.353251, 37.8775189 and -1.382425, 37.872958) as shown in Fig 3.1.

The area around River Tiva is semi-arid with a rainfall ranges from 510 mm to 1050 mm per annum, and usually occurs around May/June and with short rains in September/October. The temperature averages 14°C during the cold season and 34°C during the hot season ("Kitui County", n.d., para 15).

1.2.2 Geological Setting of the Area

The study area lies within the Mozambique belt which is characterized by the metamorphic and sedimentary rocks (Waswa et al., 2015). According to Mathu and Tole (1984), Mozambique belt stretches from the North to the South of the metamorphic and litho-tectonic domain along East Africa coast. Most of the rocks that are underlying near river Tiva are sedimentary (Waswa et al., 2015), evidenced by the existence of lateral variation which is noted by transformation of biotite gneiss into Biotite-hornblende gneiss. Also, the Tiva gneisses are classified into the following; Hornblende gneiss, Quartzo-feldspathic gneiss, Hornblende biotite gneiss, hornblende diopside gneisses, Granitoid Gneiss, Amphibolites, and Migmatites. Figure 1.1 shows the geological map of the study area.

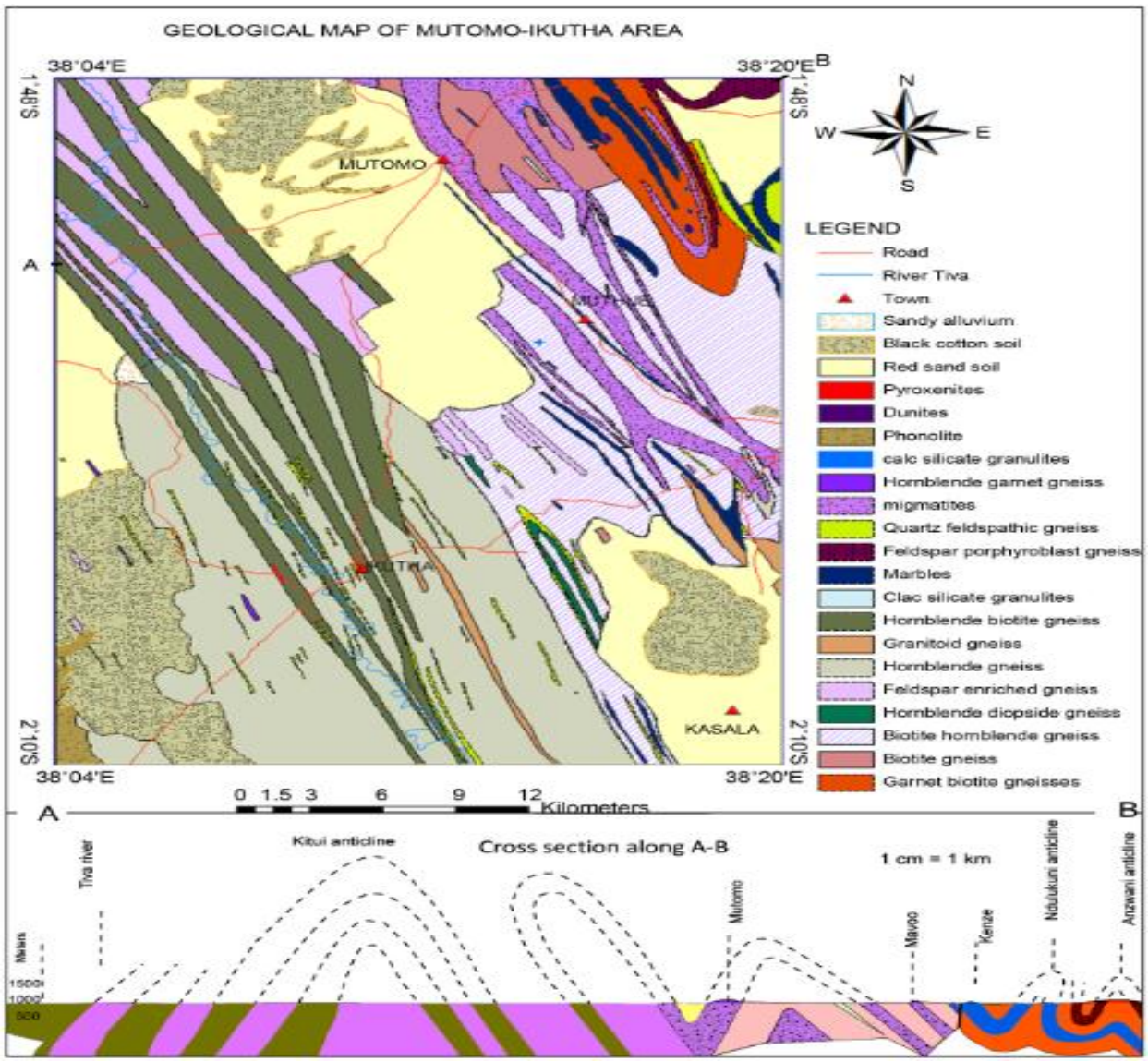

Figure 1.1: The geological map, south of the study area (Waswa et al., 2015)

1.3 Statement of the Problem

Reconnaissance surveys and geological studies in some parts of the study area indicate the possibility of heavy mineral occurrence due to the geological formation of the underlying formation of the underlying rock (Waswa et al., 2015; Mathu and Tole, 1984).

Currently, most of the river Tiva sands are harvested for construction purpose. The main challenge, however, is that no mineralogical studies have been done to establish the

mineralogical potential of the sands and as a result, there is no geochemical data for mapping of the area for mineral resources.

This study sought to characterize river Tiva sands, profiling and determine selected heavy minerals and metals associated with these sands; Ti, Zr, and Fe.

1.4 Broad Objectives

Characterization of sands for heavy minerals, profiling and distribution of selected metals along river Tiva, Kitui County, south-eastern Kenya.

1.4.1 Specific Objectives

1) To characterize the sand of River Tiva samples for element content associated with heavy minerals; Ti, Fe, and Zr;
2) To determine and profile the distribution of heavy metals associated with heavy minerals along river Tiva along the river course and across the width of the river; and
3) To determine heavy mineral sand content in the river Tiva sand samples.

1.5 Research Justification and Significance

In Kenya, data on mineral prospecting for exploitation are scarce and in practice, the potential for heavy minerals has not been fully explored.

Following the previous reconnaissance surveys and geological studies, it was identified that was there was a need to characterize the sands to determine their potential for heavy minerals exploitation. In general, heavy minerals have major economic potential as raw materials for nuclear, painting and metallurgical industry amongst others. Currently, mining of heavy minerals is undertaken in Kwale by the Base Titanium Company Ltd.

Most of the sands harvested along the river Tiva beds are used in the construction and built industry. Therefore, geochemical analyses of these sands are useful in determining the potential of heavy minerals occurrence.

1.6 Scope and Limitation of the Study

This study is limited to characterization of River Tiva sands for heavy minerals and associated heavy metals; titanium, zirconium, and iron.

A sampling of the sand samples was done along 3 Km stretch of Tiva River while sediments were sampled at a depth of up to 0.3-0.5m and subsurface (5-20cm).

CHAPTER TWO

LITERATURE REVIEW

2.1 Introduction

This chapter reviews studies related to the formation of the heavy mineral sands, various kinds of heavy mineral sands, their industrial uses and the techniques used in the characterization of the heavy mineral sands.

2.2 Sands and Formation of Heavy Mineral Sands

Sand is a mineral grain with the diameter that varies between 0.063mm and 2mm, formed as a product of mechanical weathering of the rock (De Meijer, 1998). The mineralogy of the parent rock, therefore, determines the mineralogy of the sand. Although sediments mix, when transported from the source area to the site of deposition, the mineralogy of the sand, provides reliable information on the mineral composition of the source rocks (De Meijer, 1998).

In general, there are two main types of sands; light and heavy mineral sands, based on the specific gravity method of separation, in which sand is immersed in high-density liquids such as bromoform with a specific density of 2.97 gcm^{-3}(De Meijer et al., 1990). Light sand minerals consist mainly of quartz and feldspar. Quartz is purely SiO_2 and contains little uranium, thorium or potassium. Feldspar is SiO_2, K_2O, or Na_2O and Al_2O_3 rich mineral. In the Netherlands, sand is found to have heavy minerals including garnet ($Fe^{2+}{}_3Al_2Si_3O_{12}$), rutile ($TiO_2$), zircon ($ZrSiO_4$), and, ilmenite($Fe^{2+}TiO_3$) and magnetite($Fe^{3+}{}_2Fe^{2+}O_4$) (De Meijer et al., 1990). In general, heavy minerals have a higher density than that of quartz which has a density of 2.65 gcm^{-3} (Webster et al., 2003).

Heavy minerals are derived from sedimentary rocks and found as deposits (Elsner, 2010). In general, heavy mineral sands deposits are characterized by dark colour due to its opaqueness (Elsner, 2010).

Heavy mineral grains deposition and sorting occurs in rivers, and coastal environment controlled by specific gravity, shape and size of the grain (Lener, 1997). Heavy mineral deposition and concentration occurs where the conditions are favourable hence formation of black sand deposits. In these deposits, titanium containing minerals are concentrated. According to Mason and Moore (1982), titanium is said to be the ninth most abundant crustal element at an average of 0.57%.

Gillson (1959) reported that all titanium bearing sand deposits share certain common characteristic, specifically the same source; igneous rocks or metamorphic rocks from continental land masses. Originally, none of these rocks were rich in titanium bearing heavy minerals such as ilmenite or rutile. However, because of weathering, these rocks are broken down forming a soil zone. As a result, minerals that are susceptible to weathering such as magnetite and feldspar are decomposed whereas those who were resistant; quartz, ilmenites, rutile, and zircon remain unweathered. Lastly, placer deposit is formed due to the concentration of minerals arising from erosion and transport processes.

Despite the initial similarities, there is a significant variation of the geological history of each heavy mineral deposited. According to Lener(1997), such alluvial sand may be formed in rivers, streams, coastal areas and in littoral environments. The black sands become enriched in coastal sand beach due to the following conditions; weathering, abrasion and hydraulic resulting in the breakdown of many less durable minerals such as feldspar (Lener, 1997). Principally, the wave action at the waterside sweep away minerals of less density, such as quartz, while leaving heavy minerals behind following combined processes of hydraulic sorting.

Rubey(1993) came up with the concept of hydraulic equivalence to explain the deposition of heavy minerals, now applied in most heavy mineral studies (Lener, 1997). The hydraulic equivalent grains at constant conditions is said to have same settling velocity (Tourtelot, 1968). According to Stokes' law, the velocity at which spherical particles (sand grain) settles from suspension is directly proportional to the density and the square of the particle diameter and inversely proportional to the fluid viscosity.

Therefore, due to higher density, heavy minerals are characterized by fine grain than quartz sands in the same placer (Slingerland and Smith, 1986). Also, there will be a variation in the size of the grains deposited in the same bed (Li and Komar, 1991). Some research studies have demonstrated that Stoke's law does not provide enough evidence on the size of grain distribution in the black sands deposit (Lawright et al., 1972). Lawright et al. (1972) reported the anomaly in the fineness of the heavy minerals which have low settling velocity contrary to Stoke's law of low-density minerals.

This anomaly attributes to the environment at which the heavy minerals deposits. This does not govern deposition from wind or wave breaking over fluvial or Aeolian environments which have the erosive effect. According to Slingerland (1977), there are different processes which regulate particle motion, but the most significant of them is the turbulent flow which causes the entrainment of grains. As a result, small sand particles are 'hidden' in the crevices of the large sand grains, protecting them from the action of the wave (Force, 1991). The transportation of sediments determines the conditions which affect the entrainment and settlement of grains. Therefore, for the sand grains with equal size and shape, those with higher specific gravity will not be transported further, and this is where most of the heavy minerals deposit.

2.3 Origin of the Placer Deposit and Various Types of Heavy Minerals

Black sand deposits are a class of placer ore deposit which contains high-density minerals concentrated by intense wind and wave action (Robb, 2005). The size and grade of heavy mineral sands deposit vary considerably (Robb, 2005). This mineral deposit which accumulates in the beach or river sediment as a result of weathering or erosion processes of the rock is called placer deposit. Table 2.1 shows the various minerals found in the placer deposits (Volp et al., 2009).

Table 2.1: Typical heavy minerals with associated impurities (Volp et al., 2009)

Mineral	Ideal Formula	Major Impurities	S.G
Ilmenite	$Fe^{2+}TiO_3$	Mg, Mn, V, Nb, Fe^{2+}	4.7-4.8
Rutile(Anatase-low polymorph)	TiO_2	Nb, Ta, Sn, Fe	4.2-5.5(3.8-4.0)
Pseudo rutile	$Fe^{2+}{}_2Ti_3O_9$	Mg, Mn, $Fe3^+$, Cr, OH^-	3.3-3.8
Zircon	$ZrSiO_4$	Hf, Fe, Al, U, Th	4.6-4.7
Monazite	$CePO_4$	La, Y, Ca, Th, U, Al, Fe^{2+}	5.0-5.3
Spinel	$MgAl_2O_4$-spinel	-	3.5
	$Fe^{2+}Cr_2O_4$-MagnesioChromite	-	4.4
	$Fe^{2+}Fe^{2+}{}_2O_4$-magnetite	-	5.2
	$Fe^{2+}{}_2TiO_4$-ulvospinel	-	
Tourmaline	$NaFe^{2+}{}_3Al_6Si_6B_3O_{27}(OH)_4$-schorl	Mg, Mn, Li, F^-	3.0-3.2
Garnet	$Fe^{2+}{}_3Al_2Si_3O_{12}$-almadine	Ca, Mn, Mg, Ti, Cr, Fe^{2+}, OH^-	3.5-5.3
Staurolite	$Fe^{2+}{}_2Al_9Si_4O_{22}(OH)$	Fe^{2+}, Mg, OH^-	3.7-3.8
Sillimanite	Al_2SiO_5	Fe^{2+}	3.2-3.3

In determining the source of the minerals that occur in the deposits, provenance studies are vital (Pirkle and Podmeyer, 1993). In general, the concentration of heavy minerals leads to the formation of the placer deposit. However, deposits formed on the coast are not affected when the level of the water at the sea falls **(**Pirkle and Podmeyer, 1993). Nevertheless, most of the deposits formed along the rivers or streams are altered due to the action of erosion water in the river bed, for example, the Virginia, and North Carolina deposits have undergone much alteration and erosion. Therefore, heavy mineral placer is formed where there must be a source preserving and concentrating the minerals (Pirkle & Podmeyer, 1993).

A high level of zircon mineral is associated to high concentration levels of ZrO_2. Consequently, low concentrations of TiO_2 are indicative of low mineral levels of ilmenite, leucoxene, and rutile. The desire for low Fe_2O_3 percentage restricts contaminants that contain iron such as ilmenite and magnetite while free silica requirements limit quartz content.

2.3.1 Ilmenite

Ilmenite is one of the titanium bearing mineral which is highly abundant in the earth's crust and derived from almost all intrusive and extrusive igneous rocks (Clarke, 1986). Both ilmenite and hematite have iron (Fe) in their crystal structure. At elevated temperatures, ilmenite, and hematite mix in equal proportion. In the mixture, iron (Fe) can be replaced by magnesium (Mg), manganese (Mn) and aluminium (Al). Also, titanium can be replaced by magnesium. Segregation of hematite and ilmenite to form titano-hematite occurs as temperature drops. As a result of the reaction of iron instead of titanium, the stoichiometric mass of TiO_2 content in the Ilmenite has been established to be less than 52.66 %(Clarke, 1986).

Ilmenite released from the solid rock undergoes leaching. Due to humidity, the leaching of iron occurs leading to the enriching of titanium in the mineral. As a result, there is the formation of leucoxene (Mucke and Chaughuri, 1991). This weathering process begins at the edges between two grains and only effective at the areas above the water level. The breaking of the crystalline structure of ilmenite and formation Fe/Ti oxide mixture occurs hence forming a smooth mineral crystal mainly of TiO_2. Leaching of iron oxides enriches TiO_2 leading to a reduction of magnetic susceptibility (Mucke and Chaughuri, 1991). The studies done by Temple (1966) showed that colour of the leucoxene attributes to the content of TiO_2. Table 2.2 shows the dependence of the color on the TiO_2 content (Temple, 1966).

Table 2.2: Variation of the colour with TiO_2 (Temple, 1966).

TiO_2 (%)	Color
52-63	Dark gray
63-68	Reddish gray
68-75	Auburn
75-80	Yellowish
80-85	Yellow-orange
85-90	Yellowish gray
90-95	Yellowish-white
95-100	White

Garnar (1980) found out that leucoxene calcined at temperatures of 550°C are characterized by light gray colour and are not soluble in sulphuric acid.

The process of erosion causes the disintegration of the structure of the rock leading to the exposure of the ilmenite. Most of the ilmenite is derived mainly from the igneous or metamorphic rocks. Through the process of leuconexization, TiO_2 content is increased in the ilmenite. As a result, prospecting for the mining of titanium prefer heavy mineral ilmenite during exploration (Garnar, 1980).

There is also the formation of pseudo-rutile, which is an intermediate oxidized ilmenite phase in which, a third of the Fe has leached out of the ilmenite, and all the remaining Fe oxidized to Fe^{3+}. Pseudo-rutile is Fe^{3+} TiO_9 (with 60% TiO_2). The ferric iron is leached continues and rapidly becomes Pseudo-rutile with increasing TiO_2 (Berquist, 2010). Further leaching changes Fe-rich leucoxene to become purer TiO_2 rich leucoxene (Berquist, 2010).

2.3.2 Industrial Application of Ilmenite

The most important application of ilmenite is in the manufacture of titanium dioxide (TiO_2). TiO_2 is a white pigment and is used mostly in the production of synthetic paints. Sulphate process and chloride process are the only two industrial processes used to

manufacture TiO_2. Roll process is employed where titanium tetrachloride from the chloride process used as a feedstock. Magnesium is used for separation as shown by equation 2.1

$$TiCl_4 + 2Mg \longrightarrow Ti + 2MgCl_2 \quad \ldots\ldots 2.1$$

Titanium metal and its alloys are valuable because of its low density, higher strengths at elevated temperatures and corrosion resistance. Titanium metals are also inert to the body organs, not toxic, and resistant to electric current. Therefore, used in medicine, manufacture of space of spacecraft, and nuclear industry (Elsner,2010).

2.3.3 Rutile

Rutile is the most important natural titanium dioxide of the economic value of the three crystal modifications forms. Table 2.3 shows different forms of rutile and their respective characteristics.

Table 2.3: Characteristics of Rutile and its associated minerals (Elsner, 2010)

	Rutile	**Anatase**	**Brookite**
Formula	TiO_2		
Chemistry	100% TiO_2		
Density(g/cm^3)	4.21	3.90	4.14
Mohs' scale of hardness	6-6.5	5.5-6	5.5-6
Color	Brown, foxy red, yellowish, gray beige, bluish, violet	Black, Auburn, yellowish, brown, dark blue, grey	Dark brown to green black
Magnetic properties	Nonmagnetic		
Electrostatic properties	Conductive		

In the metamorphic structure, rutile exists in the environment where it is not dependent on other minerals. TiO_2 mainly derives from metamorphic rocks composed of high levels of aluminium (Al) especially at elevated temperatures and pressure (Elsner, 2010). The chemical equations show the metamorphic processes occurring during the transformation of rutile:

$CaTiSiO_5 + Al_2O_3 \approx CaAl_2Si_2O_8 + TiO_2$ ……...2.2

$CaTiSiO_5 + CO_2 \approx CaCO_3 + SiO_2 + TiO_2$……...……2.3

$CaTiSiO_5 + O_2 \approx Fe^{2+}Fe_2^{3+} + TiO_2$……2.4

$CaTiSiO_5 + S \approx Fe_2S + TiO_2$…….……2.5

However, in migmatites and pegmatite, the occurrence of rutile is hindered and only found in granites. Rutile extraction around the world is mainly restricted to placers (Elsener, 2010).

2.3.4 Industrial Applications of Rutile

Rutile is the source of high-quality titanium and as a mineral is used in the following areas; production of metallic titanium, manufacturing of TiO_2 white pigments but only using chloride process and sheathed electrode for welding.

2.3.5 Zircon

Zircon has the chemical formula, $ZrSiO_4$ and composed of 67.22% of ZrO_2 by mass and 32.78% by mass SiO_2. It has a density of $4.68gcm^{-3}$, and it is non-magnetic, hence, cannot be identified by the magnetic tests. Zircon is colourless, yellowish, pink, brown, green, blue and black color.

In the crystal lattice of the mineral, zircon is built element with hafnium which is chemically similar. HfO_2 concentration in the zirconia mineral ranges from 0.5-2.0 % by weight. Also, zircon is reported to be radioactive due to the presence of Th and U in its structure (Elsner, 2010). According to Garnar (1984), the radiation due to Th and U cause partial disintegration of the structure lattice of the zircon leading metamictization.

This process causes the zircon to be hydrated, loose density, soften, opaque and loose colour (Vanes et al., 2002). An effect of metamictization reverses by calcination which is the most common processing step in the industry (Aral and Mcdonald, 1999).

Zircon as a deposit is formed by crystallization of the molten magma mainly from the granitic rocks. According to Garnar (1984), mineral zircon is resistant to weathering processes, and most zircon derived from metamorphic, sedimentary and volcanic rocks is due to crystallization of the zircon in the plutonites which has undergone transportation. The concentration of zircon in the placer deposit can be attributed to its ability to resist weathering and high specific gravity (Garnar, 1984).

2.3.6 Industrial Applications of Zircon

The main application of zircon is in the ceramic industry attributed to its opaque nature and whitening of the ceramic due to high refractive index, specifically in the manufacture of tiles, sanitary materials, and porcelain products. Its application has gained significance due to the high melting point, chemical purity, low thermal conductivity, flexural strength and tensile strength, corrosion resistance, wear resistance, and good tribological properties.

When zircon is decomposed at elevated temperatures or calcination of Zirconium sulphate ($ZrSO_4$) or Zirconium hydroxide ($Zr(OH)_4$), produces Zirconia (Aral and Mcdonald, 1999).

2.4 Characterization Techniques of Sands for Heavy Minerals

In general, the main components of most heavy sands are; titanium, zirconium, and iron-bearing minerals rutile, zircon, and ilmenite. The characterization of sands for heavy minerals is usually investigated using EDXRF as a major analytical technique of choice to establish the elemental composition. Reyneke and Van Der Westhuizen (2001) characterized heavy minerals of Indian sand beach using X-ray fluorescence spectrometry, optical microscopy and scanning electron microscope. He used X-ray fluorescence spectrometry to provide the elemental concentration. The fast, non-destructive nature of EDXRF analyses makes it ideal for sample characterization

(Potgieter, 2007). The structural composition of minerals is determined by XRD, using Rietveld method.

The subsequent section describes principles of each technique used in this work for characterization of the mineral sands namely; EDXRF and XRD.

2.4.1 Principle of X-Ray Fluorescence Spectroscopy

X-rays are energetic electromagnetic waves found in between the gamma and ultraviolet region of the electromagnetic spectrum. X-rays applied in conventional x- ray spectroscopy is confined to the region of approximately 0.1 to 0.25Å. The X-ray spectroscopy measurements may include emission, absorption, scatter, diffraction and fluorescence of radiation (Skoog and Leary, 1992). In principle, XRF employs the measurement of fluorescence of radiation. It is a non-destructive method which quantitatively gives the elemental composition of a wide range of materials within a short time. Due to its non-destructive nature, the requirement for preparation of the sample is minimal before analysis (Bertin, 1975).

X-rays are produced in an X-ray tube using tungsten filament (cathode) heated by an electron current passing through external filament terminals. The hot tungsten filament produces a cloud of electrons accelerated along focusing tubes towards a target material (Anode) which is Rh. The Rh anode consists of a thin film of Rh mounted on a copper block which serves to conduct heat away from the electron beam focusing point. The energetic electrons emitted by the W filament accelerate towards the Rh target following the application of potential difference between the W cathode and the Rh anode.

When the Rh target is hit by the high energy filament electrons, the inner electrons of the Rh atoms absorb this energy and the Rh atoms are excited. If the energy is sufficient to excite the inner electrons in a Rh atom, inner electrons can be expelled from the inner orbitals of the excited atom. The energy released in the form of X-rays as primary X–rays or photons originate from the Rh tube during de-excitation of the inner electrons.

This primary x-rays is used for sample irradiation, in which they are absorbed by the inner electrons in the sample atoms and dislodged from their atomic orbitals. This

dislodging process renders an atom to be in the excited state. During the deexcitation, characteristic X-rays are produced from the elements in the sample as secondary x-ray photons which cause emission of characteristic radiation (spectral lines) and this process is known as X-ray fluorescence. X-ray photons produced by the atoms of each sample element are unique in energy for each element because of the characteristic energy levels (orbitals) within the different atoms. These spectral lines are designated as K-lines, L-lines, M-lines and N-lines depending on which shell the electron vacancy fills during the de-excitation process. K_α line is emitted when an electron in L transfers to K shell (Fig 2.1).

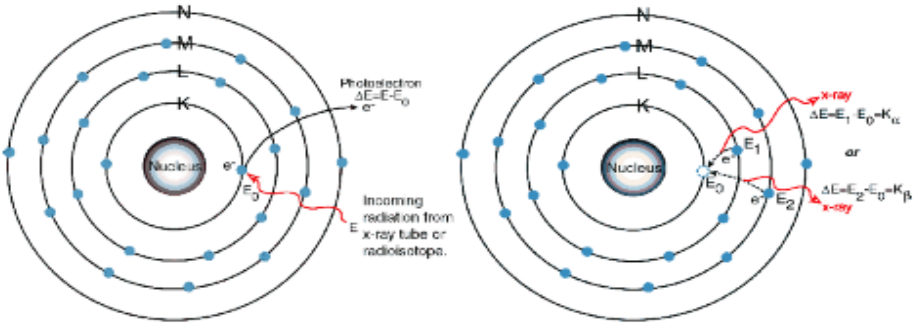

Figure 2.1: Illustration of the emission process and different energies released in the form of X-rays.

The amount of protons in the atomic nucleus and the distance of the electrons from the nucleus are directly proportional to the excitation potential of an electron in the orbital. If protons are more in the nucleus (high Z elements), and the closer the electrons to the nucleus, the stronger the electrostatic attraction between protons and the electrons. There is an electron binding energy which attracts an electron towards the nucleus. This binding energy is different for different elements and increases with increase in Z.

The absorption cross-section of the primary X-ray photon in an atom is high when the photon energy of the primary X-ray slightly exceeds the binding energy of that specific electron (Skoog and Leary, 1992).

The intensity of the characteristic secondary X-ray photons produced as spectral lines during XRF analysis can be measured with semiconductor detectors, e.g. Silicon (Li) detector for example.

Elemental concentrations can be quantitatively determined by comparing the intensities of the spectral lines produced by the sample elements with the intensities of the spectral lines produced by the calibration standards consisting similar elements of interest. The intensities of these X-ray lines are directly proportional to the concentration of the elements of interest in the analytes (Misra and Mudher, 2002).

For a particular wavelengths emitted which corresponds to sample element, the number of photons per unit time (count rate) is directly proportional to the concentration of the element in that sample (Misra and Mudher, 2002). Therefore, from the energy of the x-ray peaks, it is possible to determine the elemental composition of the samples qualitatively. Also, from the intensities of the X-ray, it is possible to quantify the concentration of the elements (Misra and Mudher, 2002).

In practice, there are two kinds of x-ray fluorescence spectroscopy; wavelength dispersive (WDXRF) and energy dispersive (EDXRF). Wavelength-dispersive X-ray fluorescence uses a crystal to separate the various wavelengths. It uses the principle of Bragg's formula, whereby the reflected wavelength for every angle of incident radiation conforms to Bragg's formula. For EDXRF, all wavelengths of incident radiation are absorbed by the semiconductor detector as an electric current proportional to the incident energy. These pulses are separated electronically using a pulse analyzer. The detector resolution and detection limit for analytes are better for WDXRF while EDXRF has the advantages of simplicity of instrumentation and less acquisition time.

A typical EDXRF spectrum will consist of multiple peaks of different intensities, each peak corresponding to a specific element in the sample. In practice, the conventional EDXRF has high detection limits up to ppm level compared to synchrotron XRF, which has up to ppb level (Falkenberg, 2002). XRF technique is usually affected by the matrix effects, consequences of sample type (thick or thin) for absorption and enhancement of analyte intensities. For thin samples, the intensity of a spectral line of a matrix M ($I_{A,}$ M) is a function of the weight fraction of the analyte, W_{AM}, the analyte line intensity from pure element standard, I_{AA} and the matrix M (Falkenberg, 2002). The equation 2.6 shows the relationship,

$I_A = f(W_{AM}, I_{AA}, M)$ 2.6

Various methods are used in solving the absorption enhancement problem. Most of these methods involve the use of the calibration standards. Quantitative analyses involve conversion of intensity data to elemental concentration by use of calibration curves or mathematical relations derived from the measurements on standards (Bertin, 1975).

2.4.2 Sands Characterization for Heavy minerals Using EDXRF

In general, EDXRF is used to determine the elemental composition of the sands in deriving the geochemical data that is used to characterize them for heavy minerals. It has applied for geochemical characterization of detrital ilmenites (Kaminsky et al., 2008). The data obtained was used to determine the source rocks of the heavy minerals. Mahanty et al. (2003) used the EDXRF data to calculate Ti/ (Ti+Fe) ratio for evaluation of the oxidation of iron oxide in the ilmenite. They used the data to explain the leaching process.

In addition, EDXRF has been used for a multi-method approach for heavy mineral exploration (Knudsen, 2005). In heavy mineral exploration, EDXRF data is used for compositional information, where the values of TiO_2 are determined. Ige and Rehren (2003) studied the black sands in South Western Nigeria using the XRF to determine the level of titanium dioxide. Kim et al. (2006) analysed the chemical composition of raw sand of the Korean beach sands with EDXRF and found Fe_2O_3 at 1.10% and TiO_2 at 0.85%. Gajah (2009) used EDXRF to determine the elemental composition of the sands at Kampung in Malaysia for heavy minerals and found out that the sediment samples contain the Ti and Fe of the elements hence the heavy minerals in the sediments were ilmenite.

2.4.3 Principles of XRD Spectroscopy for Mineral Determination

When a monochromatic x-ray beam with wavelength λ is projected into a crystalline material, the radiation interacts with the electrons in the atoms, resulting in a diffraction of the X-ray beam. The path difference between the incident and the reflected rays is $2d\sin\Theta$, where Θ is the angle of incidence and d is the spacing between successive, parallel atomic planes. For any crystal, planes exist with some orientations; each with its

specific d-spacing. Diffraction can either be due or result in constructive interference here $n\lambda=2d\sin\Theta$ or destructive in which case $m\lambda=2d\sin\Theta=0$ where $m=(n+1/2)$ with minimum intensity. Diffractions occur if the distance travelled by the X-rays reflected from successive planes differs by an integral number n of wavelengths according to Bragg's law.

$$n\lambda=2d\sin\Theta \quad \text{.....2.7}$$

By varying the angle Θ of the incident beam, the Bragg's law conditions are satisfied by some d-spacing in polycrystalline materials, by plotting the angular positions and the intensities of the resulting diffraction peaks a pattern is produced, which is a characteristic of the compound and its crystal structure. An analysis of the d- spacing and the intensity of the diffraction peaks enable determination of mineral species.

In practice, diffraction process can determine the crystal interplanar distances. It also takes advantage of differences in scattering strength between atoms to determine the position of different types of atoms within a structure. The strength with which an atom scatters radiation is given by its atomic scattering factor (f) and is proportional to the atomic number (Cullity, 1978).The value n indicates the order of reflection(n=1,2,3,4…). By using Bragg's law measuring Θ and keeping λ constant, it is possible to calculate the value of d, thus enabling determination of the crystal structure. This is the basis of XRD.

2.4.3.1 Rietveld Method

The Rietveld method helps overcome the problem in XRD interpretation of powder diffraction data due to peak overlap (Rietveld, 1969). This method assumes pattern profile refinement using a non-linear curve fitting algorithm and provides information such as the lattice parameters and position of atoms within the phase. The process is similar to a mixture of phases, where instead of a single structure added, the structures of all identified minerals in the mixture are included in the refinement, and the refinement adjusts a scaling factor which is proportional to the quantity of each phase present. Once the modeling is complete, these scaling factors can be converted to give a weight percentage of each component according to equation;

$$X_i\ (wt\%) = \frac{S_i Z_i M_i V_i}{\sum_i S_i Z_i M_i V_i} \quad \text{.....} \quad 2.8$$

Where S is the scale factor, Z is the number of formula units in a unit cell; M is the mass of the formula unit, and V is the unit cell volume (Hill and Howard, 1987).

2.4.4 Sand Characterization for Mineral Determination XRD

In general, X-ray diffraction spectrometer is used to identify the minerals. According to Rao and Misra (2009), XRD was used for precise determination of heavy minerals present in the Orissa beach placer deposit of Eastern India. According to their study, they found that there were high levels of rutile, ilmenite, magnetite and zircon. Kaminsky et al. (2008) characterized the Athabasca oil sands for heavy minerals using the XRD. They found that the oil sands contained titanium bearing minerals including rutile, anatase, brookite and ilmenite. Also, Nallusamy et al. (2013) used X-ray diffraction technique to study sand of the Thathapally-Kayamkullam. They found that the sand consisted of ilmenite, sillimanite, zircon, garnets, rutile, monazite and magnetite. XRD analysis of sand supported the idea that there had been alterations leading to high titanium dioxide concentration. Recovery of ilmenite and other minerals studies of Teri sands of Tamul Nadil, India (Babu and Rao, 2009. They used XRD to identify the minerals present in Teri sands and concluded that out of the total heavy minerals present; ilmenite accounted for 3.7%.

CHAPTER THREE

MATERIALS AND METHODS

3.1 Introduction

In this chapter, the study area is described in addition to the sampling methods used. The chapter also describes the analytical techniques used in the determination of the elemental composition of the heavy mineral sands and as well as XRD techniques for mineralogical studies.

3.2 Description of the Study Area and Sampling Method

Kitui town is located about 165 km East of Nairobi and bound by latitudes 1^0 00' and 1^0 30' S and longitudes 38^0 00' E. Geographically, the study area is located to the west of Kitui town where there are much of reduced remnants of an older erosion cycle deeply above the deeply dissected sub-Miocene peneplain (Sanders, 1954). The study area is at Kwa-Vonza location in Kitui County, and the river Tiva flows southwards.

3.2.1 Sampling of River Sediments

Sampling was done along river Tiva in Kwa Vonza, specifically at; Kalimbevo, Nduumoni, and Tanganyika area. River Tiva flows southwards, and Mwita Syano and Mikuyuni are the main tributaries.

The following are the sampling materials used;

a) Soil Auger
b) GPS device
c) Shovel
d) Sampling bags, labels and masking tape
e) Notebook, pen and permanent marker.

Ten sampling sites along river Tiva were identified, whereby for each sampling site, was identified using Global Positioning System (GPS) (Appendix 1) using Garmin

GPSMAP®64 model. The sampling for sediments was done from the main river bed along river Tiva at a stretch of 3 Km and approximately 400-500 m wide from each other. All these sites were sampled between 3rd and 5th June 2012. Table 3.1 and Figure 3.1 shows the sampled sites.

Table 3.1: Sampling areas with corresponding sampled sites.

Sampling areas	Sampled sites
Kalimbevo	T1, T3, T5
Nduumoni	T7, T9, T11
Tanganyika	T13, T14, T15, T16

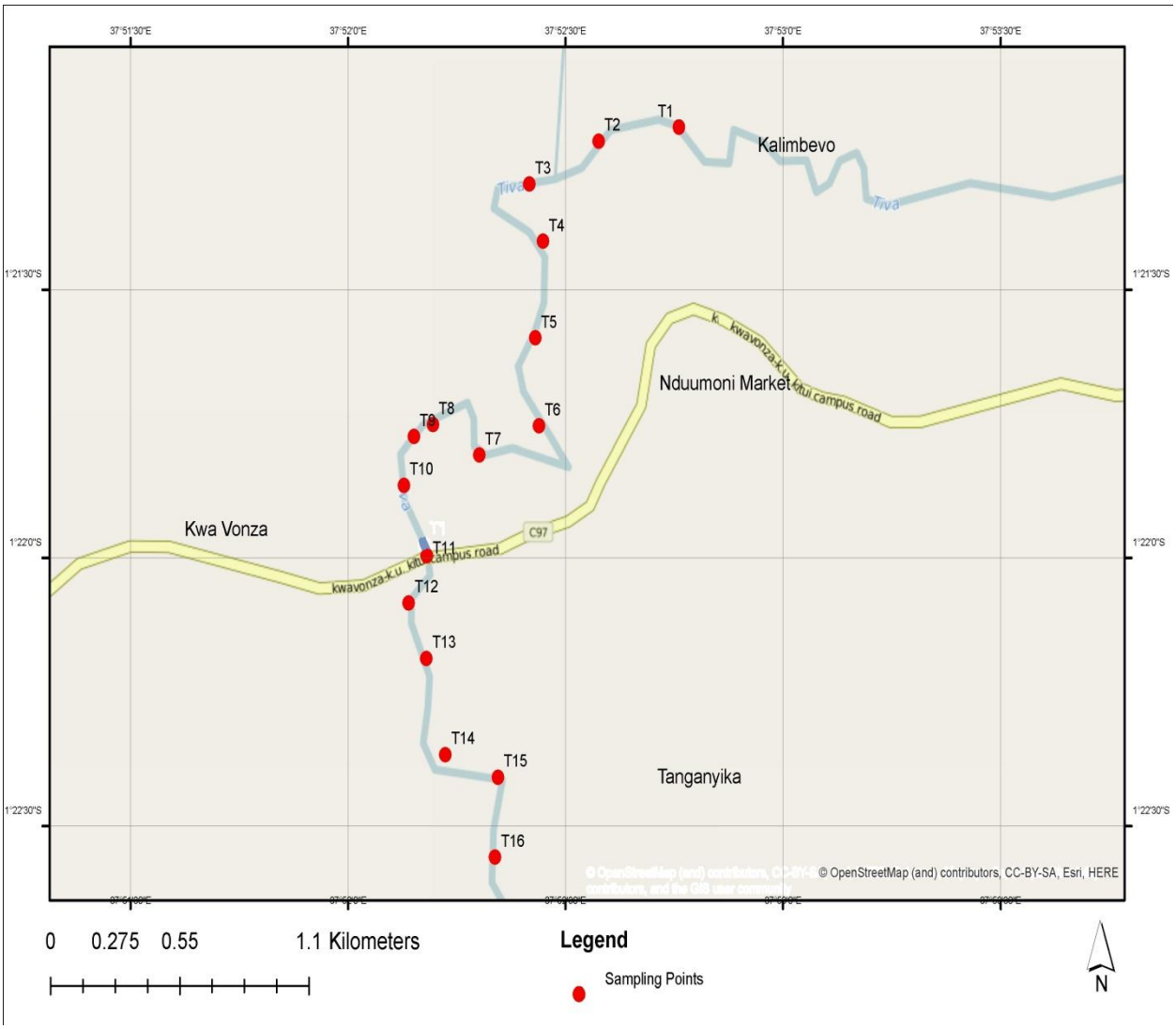

Figure 3.1: Field sampling site locations

About 0.5kg of sand samples in duplicate was sampled from each sampling site at different depths;0-10cm and 30-50cm using hand auger (Hamzah et al., 2009). River sediment samples were collected directly using the auger at a depth ranging from 0-50cm below the river bed. All of the samples were collected at an interval of 400m, at the right, center and left of the river bed, for each site (Fig 3.2 & Fig 3.3).

The sampling locations were identified from Tiva bridge, 2 Km upstream and 1Km downstream from the bridge and labeled as; T which represented river Tiva, followed by the site number (e.g. 1,2,3…). Consequently, the position of the sampling location (right, Centre and left represented by R, C, L respectively) and finally profiled depth(0 cm and

50 cm representing subsurface and 50cm deep respectively). For example, the sample collected at the location site 1 on the right side of the river bed at the subsurface was labeled as T1R0.

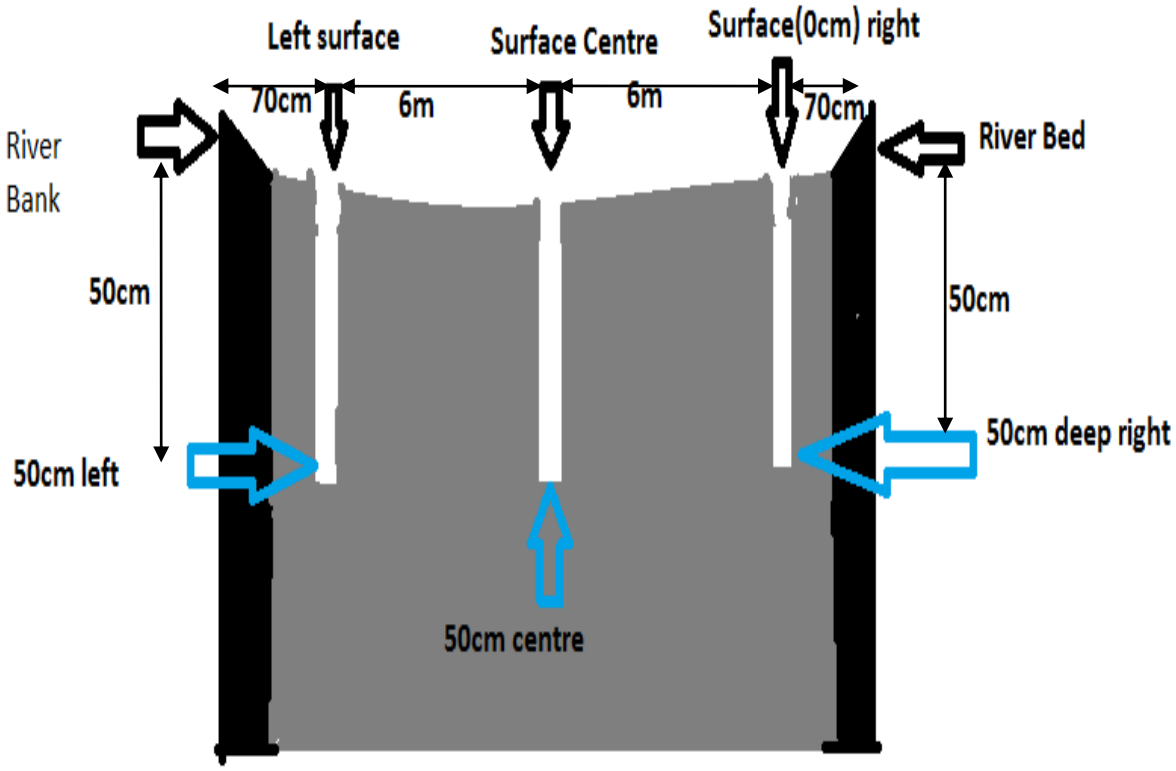

Figure 3.2: The river bed profile of sampling (approximate distances)

Each sample was packed in a polythene bag and labeled accordingly for laboratory analyses. A total of 47 samples sampled for this study.

Figure 3.3: Black sands in river Tiva

3.3 Sample Preparation for EDXRF Analyses

Prior to EDXRF analyses, the sands samples were sieved to grain sizes less than 2mm and ground to microscopic particles 75µm using the pulveriser following oven drying to constant weight (Osan et al., 2002) at the Department of Materials and Testing Research laboratories. The fine powder obtained was packed in a labelled polyethene bag for further preparation for EDXRF analysis (Figure 3.4).

Figure 3.4: The pulveriser assembled for the process

Sample aliquots were mixed with starch binder in ratios (2-5) used to determine the dilution factors and were homogenized using mortar and pestle (Mori et al., 1999).

The resulting mixture aliquots were pelletized into a thin pellet with diameter 2.5 cm at 30 KPa and weights determined before EDXRF analysis. For each sample, triplicates of thin pellets weights between 0.3-0.5 grams were prepared for EDXRF analysis, specifically for Ti, Fe and Zr concentration determination.

3.4 Quantitative Energy Dispersive X-ray Fluorescence Analysis

An XRF-spectrometer used consisted of the X-ray tube (generates primary X-rays to excite atoms in the sample), collimators (to focus X-rays on the crystal and detector) and the semiconductor detector. In this study, Energy dispersive X-ray fluorescence spectrometer used was Shimadzu model series EDX-800HS, available the Department of Material Testing and Laboratories. Figure 3.5 shows the EDXRF spectrometer used in this study.

The EDX-800HS spectrometer used consisted of the following modules;

1. X-ray generator unit which consists of an x-ray tube of side window type and with a Rh target with the power of 50W, operated with a power of 5-50KV and current of 1-1000μA. In addition, there are primary x-ray filters which automatically exchange between 5 types; Al, Ti, Ag, Mo, Ni and Mo.

2. A Si (Li) detector, supplied with liquid nitrogen at the time of analysis, consuming about 1L/day.

3. Counting Unit and control unit producing pulse shaping signal from a digital processor with a measurement range 0-20, 0-40(KeV).

4. Sample and measurement compartment consist of automatic opening and closing cover that goes up and down with each measurement. The measurement compartment has irradiation diameter of 10mm.

5. EDX workstation that controls the instrument during the analysis with a data processing unit for qualitative and quantitative measurements.

The samples were measured in air and irradiated for 50 seconds. The samples were analysed within 10mm diameter for the radiation exposure. The elemental sensitivity was determined from the measurements of single element samples. The sample absorption effects were corrected using thick target containing Mo (Anjos et al., 2000).

The spectra generated were evaluated for intensities by non-linear least square fitting software called AXIL (Analysis of X-Ray Spectra Interactive Least Square Fitting) and QAES (Quantitative Analysis of Environmental Sample) software from the IAEA, and available at he Institute of Nuclear Science and Technology, University of Nairobi were used for quantitative analyses.

Figure 3.5: EDXRF spectrometer used in this study

3.4.1 Determination for Detection Limits for EDXRF analyses

The lower limit of detection is the concentration equivalent to three standard counting errors (Bertin, 1970), of a set of measurements of the background intensity (Jenkins and Gilfrich, 1992).

In this study, the lower limit of detection was determined for pelletised soil sample of a standard reference PTXRF-09. The values calculated by using equation 3.1 (Mangala and Patel, 1995).

$$LLD = \frac{3}{m}\sqrt{\left(\frac{R_b}{T_b}\right)} \qquad \ldots\ldots\ldots\ldots\ldots\ldots\ldots\ldots\ldots\ldots\ldots\ldots\ldots\ldots\ldots\ldots \quad 3.1$$

Where R_b is the background count rate, T_b is the background count time and m is the sensitivity of the instrument. LLD equation provides a theoretical limit of determination, which is lower than the expected in real samples. It is dependent on the matrix of the sample used to determine the LLD.

3.5 Sample Preparation and XRD Analyses

Sample preparation for XRD analysis followed a protocol developed by ICRAF (Nyambura et al., 2014). This procedure aimed at achieving the following conditions; indiscriminate, homogeneity and grain size reduction for coarse samples like sand to enhance reproducibility and repeatability (Nyambura et al., 2014). Reduction in size and homogenization of samples achieved by 12minutes wet milling of 3g air dried and 2mm sieved sand sample in McCrone micronizing mill with ethanol as grinding fluid. The mixture was then centrifuged for 10 minutes and decanted. Consequently, hexane added to the sample in the ratio of 0.5 ml hexane to 1 gm of the sand sample. After mixing, the sample was dried at 80 °C in an oven and sieved to 250 μm particle size (Nyambura et al., 2014). This procedure provided optimum conditions for XRD mineralogical analyses. Powder crystals in random orientations allow goniometer to swing through many angles ensuring the necessary quantity of crystals and diffraction angles to determine mineralogy (Nyambura et al., 2014).

3.5.1 Analyses with XRD Spectrometer

The XRD analysis was performed using Bruker benchtop, D2 phaser diffractometer system. It has Ni-filter and Cu K_α radiation generated at 30 KV/10 mA. The detector is the scintillation counter 1-dimensional LYNXEYE with a maximum usable range of -3 to 160° at 2θ. The spectrometer operates at a power supply of 90-250V, has inbuilt computer for control of operations, data acquisition and processing.

X-ray diffraction analyses were done at International Center for Research in Agroforestry (ICRAF) laboratories; samples scanned at 2θ. The XRD patterns recorded at a variable rotation of 15° in the angular measurement range of 3° to 75° (Nyambura et al.,2014).

Diffraction pattern obtained was analysed using the Powder Diffraction File(PDF) database from the International Centre for Diffraction pattern (ICDD). The position and the relative intensity of a series of peaks were used to match experimental data from the diffractogram to the patterns in the database. The concentration of the mineral composition of sand samples was semi-quantitatively determined using a ratio of peak intensities as a function of weight fractions for any two phases in a mixture (Nyambura et al.,2014).

3.6 Determination of Oxides of Elements of Interest

Elements of interest of the heavy mineral sand were converted to their respective oxides using a model developed by Berquist, 2010. Appendix 2 shows the model used in conversion.

3.7 Fe/Ti Ratio Determination

Fe/Ti ratio was used to determine for evaluation of titaniferous minerals (Martin & Long, 1960), and to evaluate the enrichment of titanium bearing heavy minerals, in this study.

3.8 Principal Component Analysis

Principal component analysis was performed on the data of the results of the concentration of the selected elements; Ti, Zr, Fe, V, K, Ca, Mn, Cu, Zn, and Sr using XLSTAT software to get a clustering of the elements and to identify the correlations amongst the samples.

CHAPTER FOUR

RESULTS AND DISCUSSION

4.1 Validation of the EDXRF measurements

4.1.1 Results of EDXRF Analyses of Certified Reference Material

Certified reference material (CRM) from IAEA, PTXRFIAEA-09 river clay soil sample was analysed to determine the accuracy of the analytical method used in this study. The results obtained were compared with certified values (Table 4.1).

Table 4.1: Results of Certified Reference Material (PTXRFIAEA-09)

Element	Experimental Mean values (µg/g)	Certified values (µg/g)	Deviation error (%)
Ti	4100±100	4300±200	-4.65
Fe	25700±1200	29700±4100	-13.47
Zr	290±30	302±2	-0.66

The results show the deviation to within the 15% or better for most of the elements analysed.

4.1.2 EDXRF Determination of Lower Limits of Detection

Table 4.2 shows the results of the EDXRF detection limits obtained for the elements of interest in this study, following analyses of PTXRFIAEA-09.

Table 4.2: Results of EDXRF detection limits of the soil sample

Element	LLD value(µg/g)
Ti	76
Fe	20
Zr	2.8

The detection limits for elements of interest in this study were found to decrease with increasing atomic number. Zirconium had lowest value for detection limit at 2.8µg/g. These values are consistent with those published elsewhere (Mangala and Patel, 1996), typical for analyses of soil samples with EDXRF. The Si (Li) detector resolution measured at 180eV for Mn Kα (5.9KeV).

4.2 Characterization of River Tiva Sands for Heavy Minerals

In general, the heavy minerals are predominantly present in sedimentary rocks in a small amount as compared to light minerals. Light minerals are associated with silicates, sulfates, sulphides, phosphates, carbonates and mica (Hollyer et al., 1999). Formation of HM from their parent rocks by weathering of resistant minerals, show relative concentrations and that non- resistant to weathering decrease in abundance as swept away (Dryden and Dryden, 1946). Characterization of HMS followed EDXRF analyses of the sand samples to determine the mineralogical composition.

4.2.1 Elemental Determination of the Sands for Heavy Minerals

The heavy mineral assemblage influenced by three kinds of processes such as physical sorting, mechanical abrasion and dissolution which result in partial or total loss of minerals from the parent sediments during sedimentation (Morton and Hallsworth, 1999).

The elemental contnent of the sands were determined by EDXRF analyses after the sand fractionalization. The EDXRF analyses of this fractionalization provided a reliable

estimation of the elements (Ti, Zr, and Fe) composition. Results of these elemental compositions are presented as oxides after conversion using the Berquist model (appendix 2 & 4). In general, 47 composite samples were analyzed for Ti, Fe, and Zr composition. Table 4.3 shows a summary of averages of results of EDXRF analyses of 47 samples from ten sampled site locations in Appendix 3.

Table 4.3: Elemental results of the River Tiva sands in µg/g by weight

Elements	**Mean (µg/g)**	**Minimum (µg/g)**	**Maximum (µg/g)**
Fe	73135±6027	1475±233	215333±46918
Ti	22976±1971	62167±784	72667±18626
Zr	1115±136	220±42	4427±285

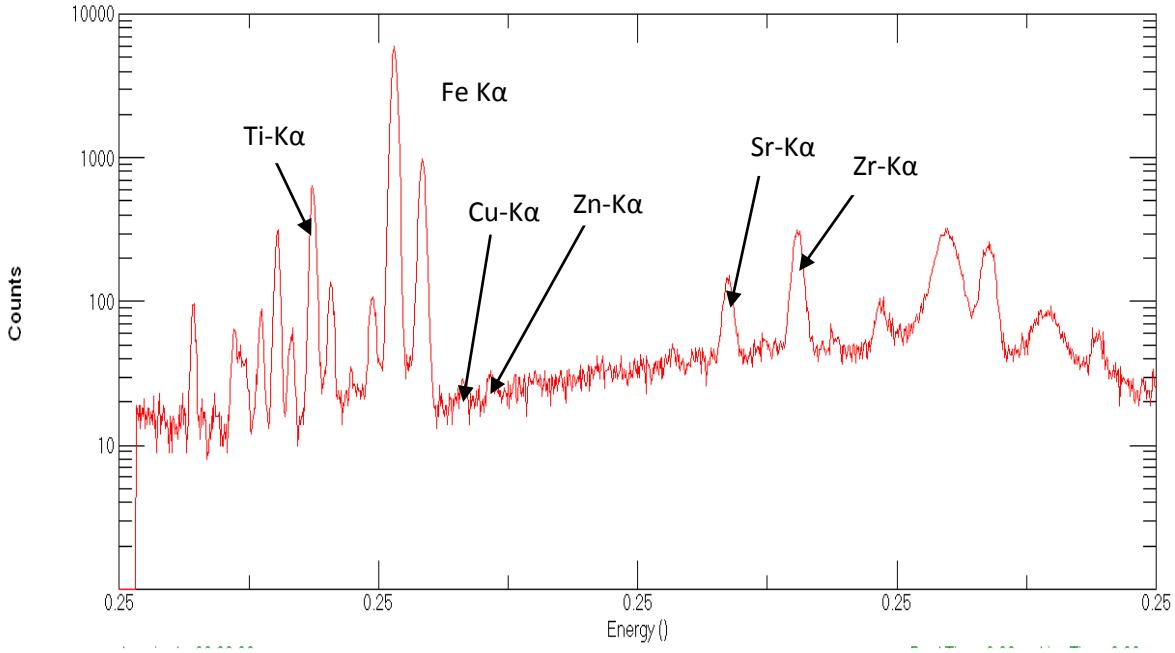

Figure 4.1: Typical EDXRF spectrum of sample T15R01

Fe was found to be dominant in the samples and averages (73135 ± 6027) µg/g followed by Ti with (22976 ± 1971) µg/g and finally followed by Zr with the concentration of (1115 ± 136) µg/g

Figure 4.2 shows the correlation between the two elements; iron and titanium with (r^2=0.9381), which is indicative of the significant amount of titanomagnetite derived from mafic rocks (Volp et al., 2009).

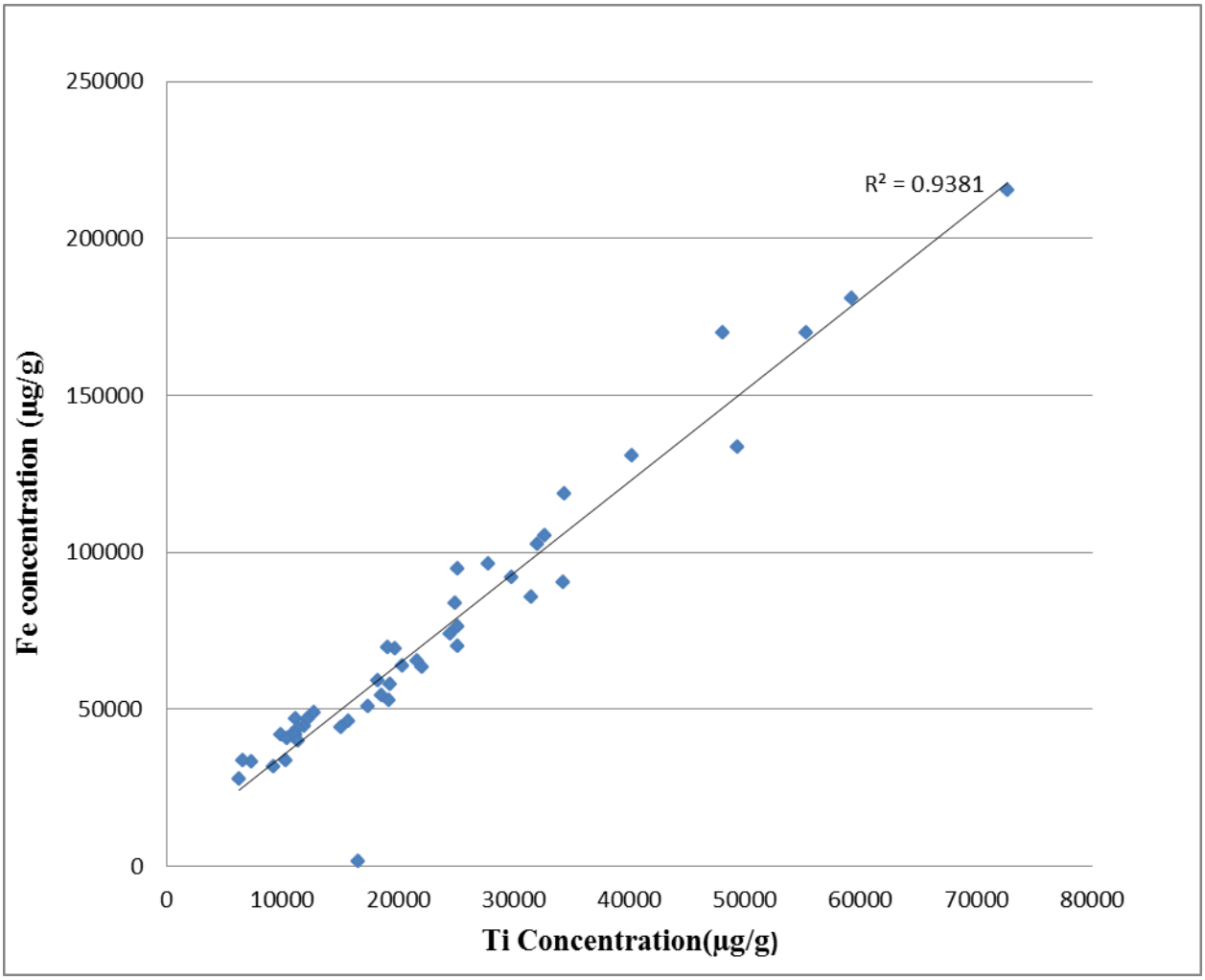

Figure 4.2: Correlation between Fe and titanium in river Tiva

Table 4.4 shows that results obtained for hematite (Fe_2O_3) as the dominant mineral oxide with 10.46% in the Tiva sands, rutile (TiO_3) (3.83%) and (ZrO_2 (0.15%) respectively. In general, TiO_2 is associated with the heavy minerals such as rutile while Fe_2O_3 is associated with the heavy minerals such as hematite (Berquist, 2010). The zirconium bearing oxides occur as $TiZrO_2$ and Baddeleyite, which occur as ZrO_2.

Table 4.4: Oxides found in the river Tiva sediments (n=47)

Oxide	Mean (%) Concentration	Standard deviation (%)	Minimum (%)	Maximum (%)
Rutile(TiO_2)	3.83	2.43	1.04	12.12
Hematite(Fe2O3)	10.46	6.26	0.21	30.79
Baddeleyite(ZrO2)	0.15	0.13	0.03	0.60

Figure 4.3 shows the variations of the oxides that associated with the heavy minerals in river Tiva sands.

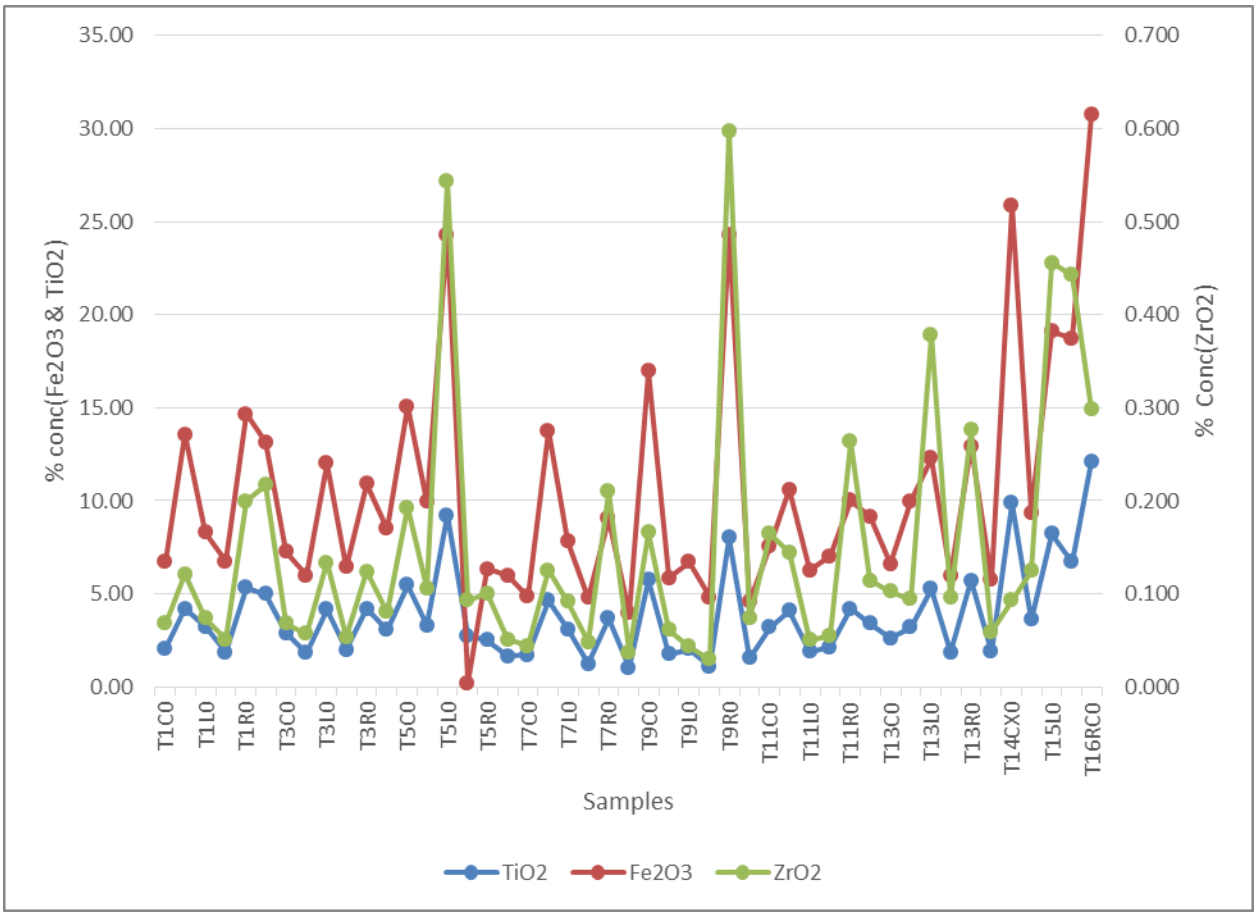

Figure 4.3: Concentration of oxides associated with HMS

4.3 XRD Mineralogical Analyses

Table 4.5 and Figure 4.4 show the results of the XRD analysis of selected ten samples analysed in this study. The XRD analyses results obtained indicate that the Tiva sands are mainly composed of Albite and Quartz in estimated proportion of 23% and 40% respectively. Other minerals include; ilmenite (4%) and hematite (7.99%) summarized from the results of analyses of 10 selected samples (Appendix 5).

Figure 4.5 shows the typical XRD diffractogram of the samples analysed in these study. The titanium bearing minerals can be attributed to the presence of ilmenite in the samples. Also supported by the correlation between the Fe and titanium in the sand samples (r^2=0.9381). The Zirconium bearing minerals were not detected in the selected samples analyzed.

Table 4.5: XRD analyses results of the River Tiva sands

minerals	Mean (wt %)	Std	min	Max
Albite	23.78	3.65	20.13	27.43
Diopside	0.95	3.00	0.00	3.95
Hematite	7.99	6.12	1.87	14.11
Hornblende	7.5	5.81	1.69	13.31
Ilmenite	4.09	5.55	0.00	9.64
Microcline	4.19	8.85	0.00	13.04
Orthoclase	7.95	7.07	0.88	15.02
Quartz	40.33	11.73	28.60	52.06
Tremolite	3.22	5.21	0.00	8.43

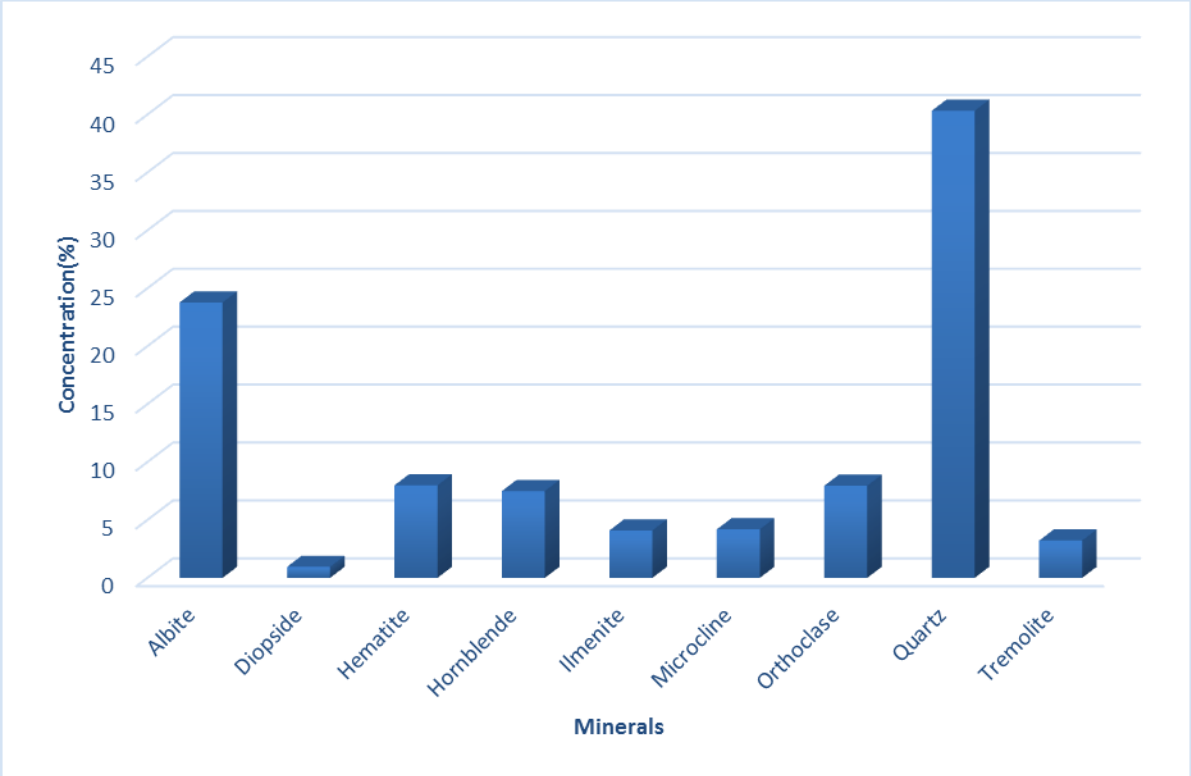

Figure 4.4: Mineral variation in Tiva sand

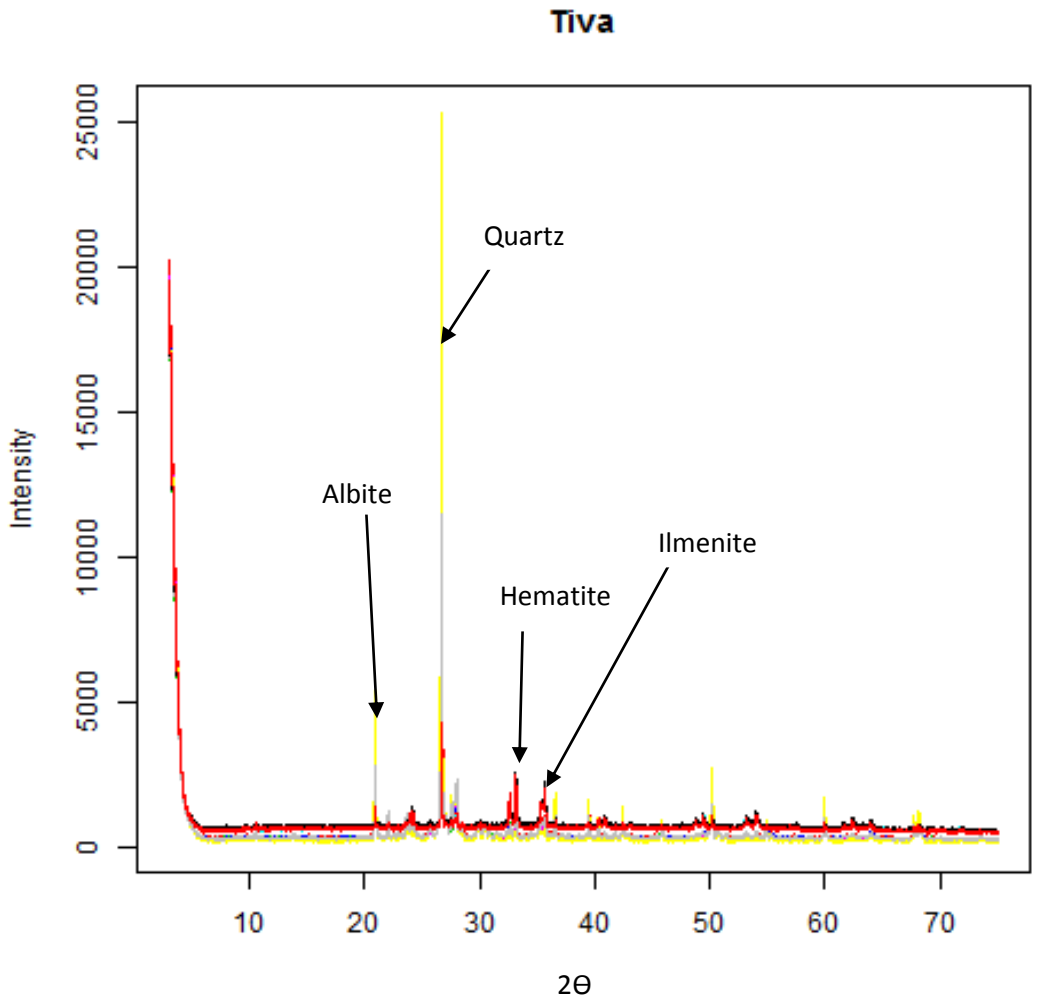

Figure 4.5: Typical diffractogram for river Tiva sand samples

4.4. Distribution of Zirconium in Sand Samples

Figure 4.6 shows the distribution of Zr in sand samples analysed in this study (Appendix 6). High levels of zirconium were recorded in site T5, T9, T14 and T15, which is indicative of zirconium bearing minerals (Zircon), located at the subsurface (1529 µg/g) but lower at profiled depth of 50cm (593 µg/g). Also, because Zr is resistant to erosion and leaching, hence it can be carried down the bed. These sites are indicative of potential zircon mineralization.

In general, Zr concentration is high at the right-hand side of the river except at convex of the river bed where more deposition (T5 and T15).

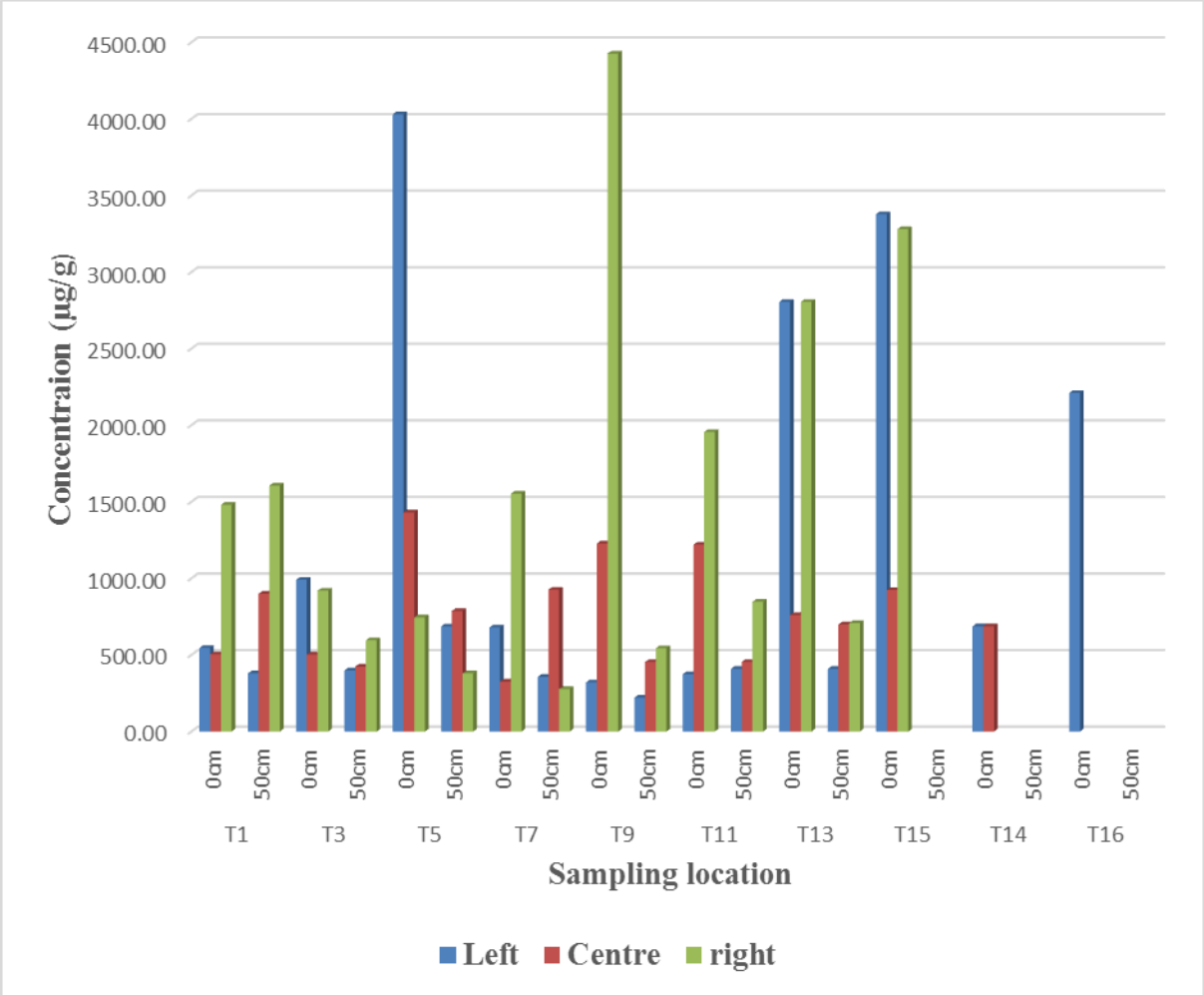

Figure 4.6: Distribution and depth profiling of zirconium in river Tiva samples

4.5 Distribution and Depth Profiling of Titanium.

Figure 4.7 show the distribution and depth profiling of titanium in river Tiva sand samples. In general, the results show high titanium concentrations at the subsurface. The average concentration level of titanium on the surface is 34033µg/g compared with 14625µg/g at the depth of 50cm (Appendix 7). This is because heavy minerals are resistant to erosion and leaching.

ANOVA analysis was done to determine any significant differences in the concentration of the three points sampled on the river bed (right, center and left). In general, from the results obtained it was found there was no statistical significant difference in the values of

the concentration across the river bed with the p-value 0.7 at 95% confidence level for most samples analysed except for river convex sites(T5, T13 and T15).

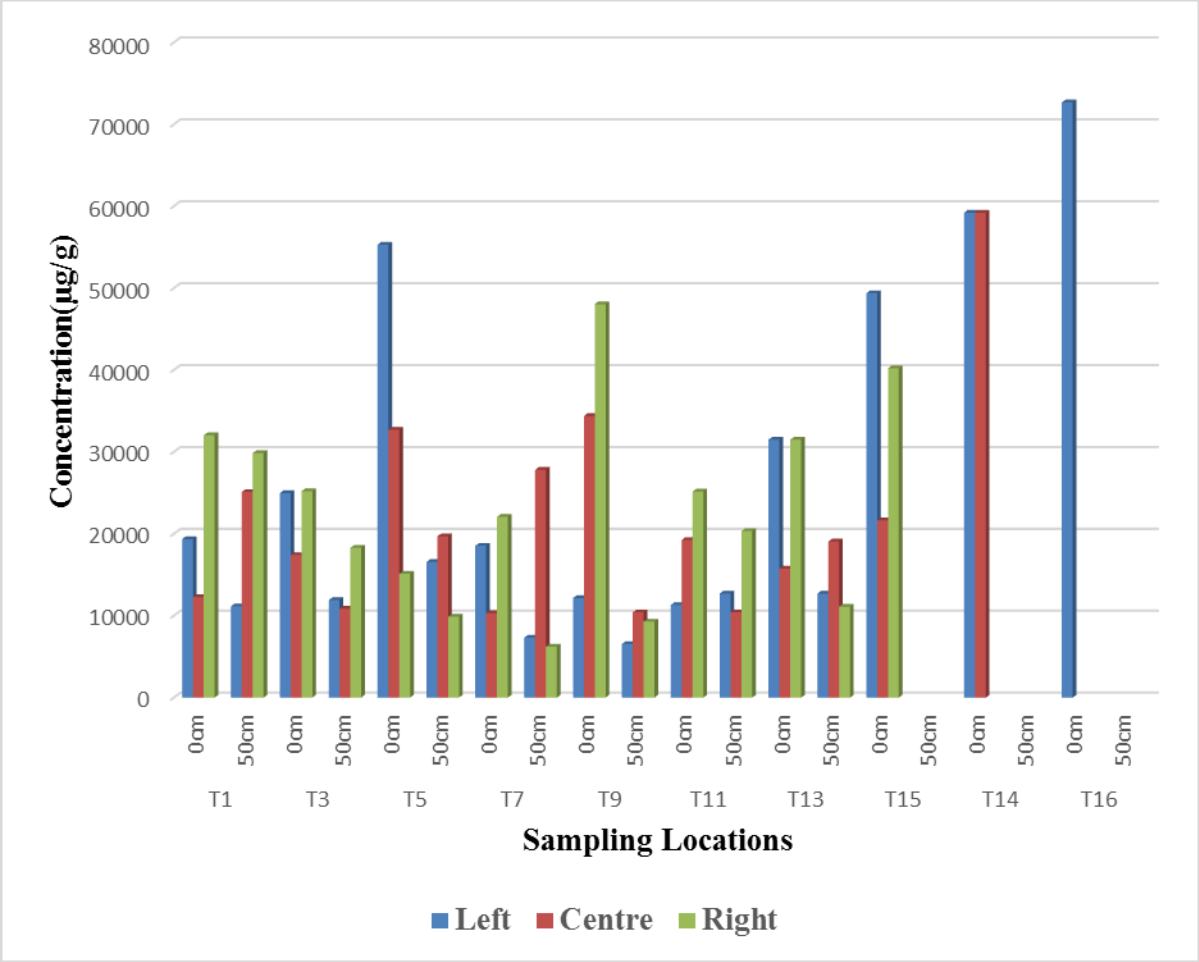

Figure 4.7: Distribution and profiling of titanium in river Tiva sand samples

4.6 Iron Distribution and Depth Profiling of Iron in River Tiva Bed

Distribution of Fe in the samples was studied across river Tiva, by comparing the results obtained for samples on the right, center, and left of the riverbed downstream. Figure 4.8 shows that the concentrations of iron across the river as evenly distributed, and there was no significant difference of the concentration values in the sample locations (right, center and left) following ANOVA analysis (p-value was 0.7 at 95% confidence level) except at the convex (T5, T9 and T14).

The results indicate that most of the Fe are concentrated on the surface of the river bed with an average of 104328µg/g in comparison to the depth of 50cm at 51016µg/g (Appendix 8).

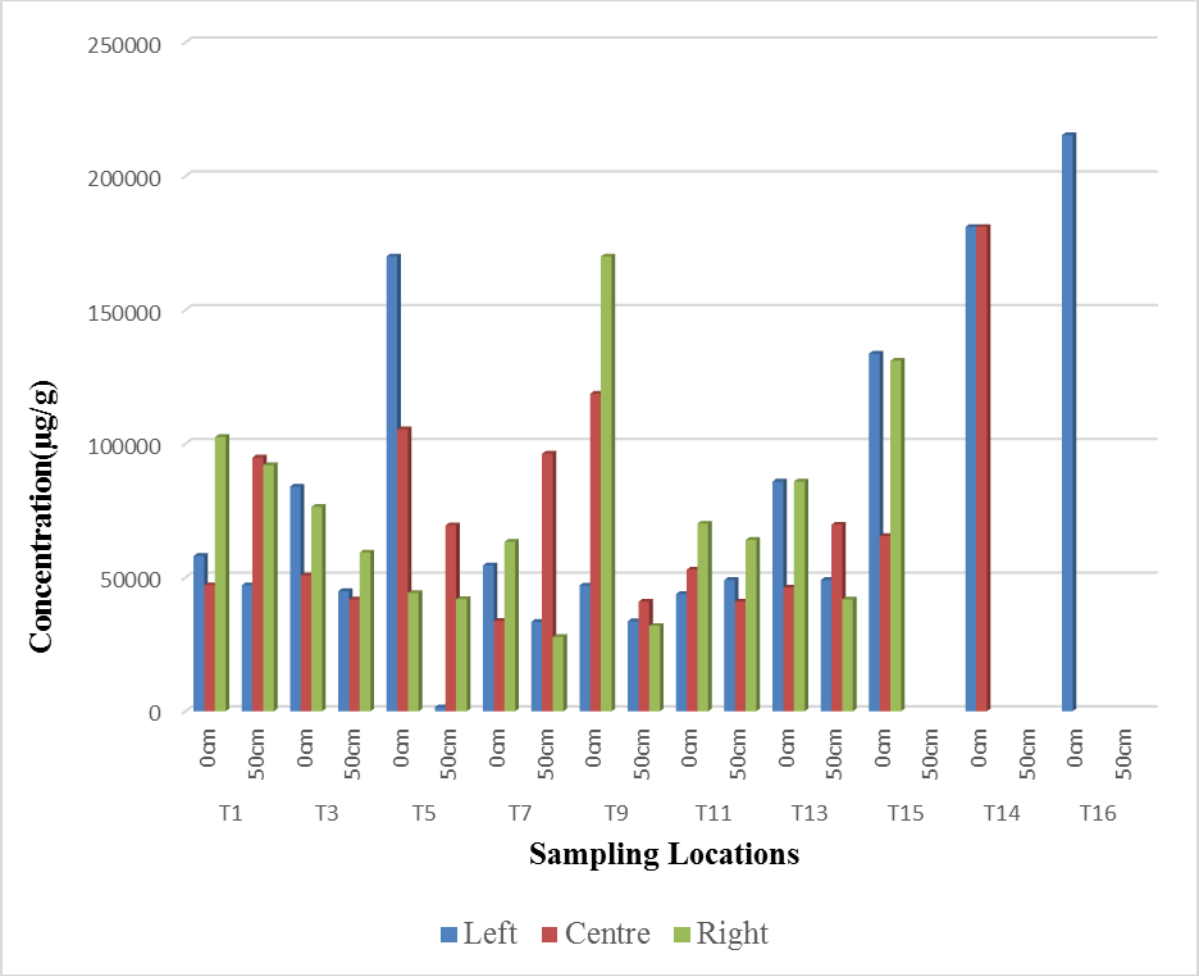

Figure 4.8: Distribution and profiling of Iron in river Tiva sands

4.7 Distribution of Heavy minerals along the River

The results in Table 4.6a, 4.6b, and 4.6c show the distribution of the elements of interest in this study in the sampled areas: for Kalimbevo; Ti-21530±1841µg/g (9870 µg/g-55300 µg/g), Fe-68400±5547 µg/g (1475 µg/g -170000 µg/g), and Zr-961±133 µg/g (379 µg/g -4030 µg/g). Nduumoni area; Ti-18126±1361 µg/g (6217 µg/g-48033 µg/g), Fe-61410±4636 µg/g (27733 µg/g-170000 µg/g), and Zr-995±108 µg/g (220 µg/g-4427 µg/g). Tanganyika area; Ti-33279±3182 µg/g (11100µg/g-72667 µg/g), Fe-100068±7706

µg/g (40067 µg/g -215333 µg/g), Zr-1630±187 µg/g (438 µg/g -3377 µg/g). Tanganyika area had high levels for most elements (Table 4.6a, 4.6b, and 4.6c). Specifically, site T16 registered high concentration values of titanium (72667±18626) µg/g attributed to deposition of heavy minerals.

Table 4.6a: Concentrations of elements of interest in µg/g from Kalimbevo area (n=3, µ±1δ)

Sample	Ti	Fe	Zr
T1C0	12250±1060	47100±3818	504±91
T1C50	25100±1555	94850±5444	899±124
T1L0	19350±2192	58050±7424	546±77
T1L50	11150±353	47100±565	379±42
T1R0	32033±1739	102533±6576	1480±251
T1R50	29850±1909	92000±2969	1605±304
T3C0	17400±2058	50800±5488	503±42
T3C50	10845±1916	41800±3818	423±38
T3L0	24950±2475	83950±9263	991±56
T3L50	11900±1609	44867±5774	399±99
T3R0	25200±1682	76400±5828	920±84
T3R50	18300±794	59333±3288	596±123
T5C0	32700±6155	105400±19028	1430±314
T5C50	19700±1273	69500±4384	787±21
T5L0	55300±4384	170000±12727	4030±495
T5L50	16550±1202	1475±233	686±135
T5R0	15100±141	44150±494	745±70
T5R50	9870±646	41900±2720	379±25
AVERAGE	**21530±1841**	**68400±5547**	**961±133**
MIN	**9870±646**	**1475±233**	**379±42**
MAX	**55300±4384**	**170000±12727**	**4030±495**

Table 4.6b: Concentration of elements of interest in µg/g from Nduumoni area (n=3, µ±1δ)

Sample	Ti	Fe	Zr
T7C0	10315±544	33800±707	326±51
T7C50	27800±4101	96250±15202	926±190
T7L0	18533±227	54533±4760	679±108
T7L50	7320±321	33367±802	356±26
T7R0	22067±723	63333±3635	1553±302
T7R50	6217±784	27733±4460	277±75
T9C0	34367±3099	118667±9237	1227±25
T9C50	10407±710	40933±4234	454±59
T9L0	12150±1627	47000±3677	320±56
T9L50	6537±717	33667±4479	220±42
T9R0	48033±1305	170000±5568	4427±285
T9R50	9273±863	31900±1609	543±59
T11C0	19233±1222	53000±3610	1220±95
T11C50	24533±1401	74200±3799	1072±133
T11L0	11300±990	43800±6364	374±60
T11L50	12700±458	49067±1986	409±43
T11R0	25150±778	70100±3536	1955±262
T11R50	20333±2593	64033±5777	847±72
AVERAGE	**18126±1361**	**61410±4636**	**955±108**
MIN	**6217±784**	**27733±4460**	**220±42**
MAX	**488033±1305**	**170000±5568**	**4427±285**

Table 4.6c: Concentration of element of interest concentrations in µg/g of Tanganyika area (n=3, µ±1δ)

Sample	TI	FE	ZR
T13C0	15750±636	46250±3182	760±161
T13C50	19067±2710	69767±8479	699±106
T13L0	31500±707	85900±3253	2805±346
T13L50	11100±728	41800±2710	707±46
T13R0	34267±737	90467±2854	2047±266
T13R50	11300±953	40067±3092	438±95
T14CX0	59200±3860	181000±1170	687±85
T15C50	21650±1768	65500±7	924±97
T15L0	49367±1665	133667±4619	3377±215
T15R0	40200±2610	131000±8490	3280±213
T16RC0	72667±18626	215333±46918	2210±428
AVERAGE	**33279±3182**	**10.01±0.66**	**1630±187**
MIN	**11100±728**	**40067±3092**	**438±95**
MAX	**72667±18626**	**215333±46918**	**3377±215**

Figure 4.9 shows a variation of the distribution of the three elements downstream the river. However, Fe and Ti increase downstream. High anomalies observed at site T5 and T9 represents a section of river meanders whereby there is high deposition at the convex of the river bed. At these points, however, surface analyses (i.e. at 0-10cm) indicate high concentration levels of Fe, Ti, and Zr (Fig 4.9).

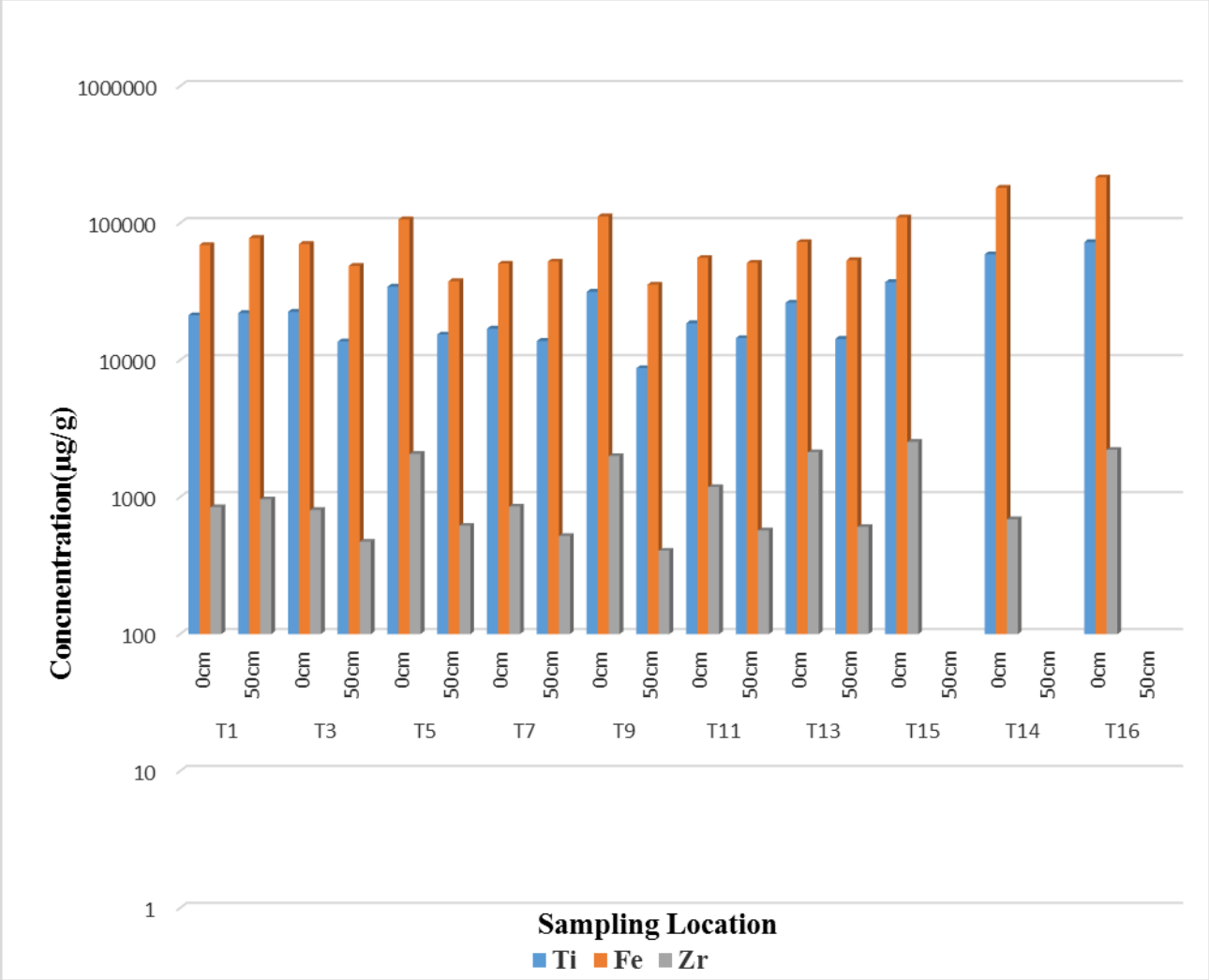

Figure 4.9: Depth profiling of heavy minerals distribution along the river Tiva

4.8 Fe/Ti Ratios

Fe/Ti ratio is usually determined for evaluation of titaniferous minerals (Martin & Long, 1960). Samples with high Fe/Ti ratios >1 are considered strongly ferromagnetic titanomagnetite.

Figure 4.10 shows Fe/Ti ratios for all samples analysed with EDXRF. In general, all the samples analysed are characterised by strong ferromagnetic titanomagnetite typical of heavy mineral sands.

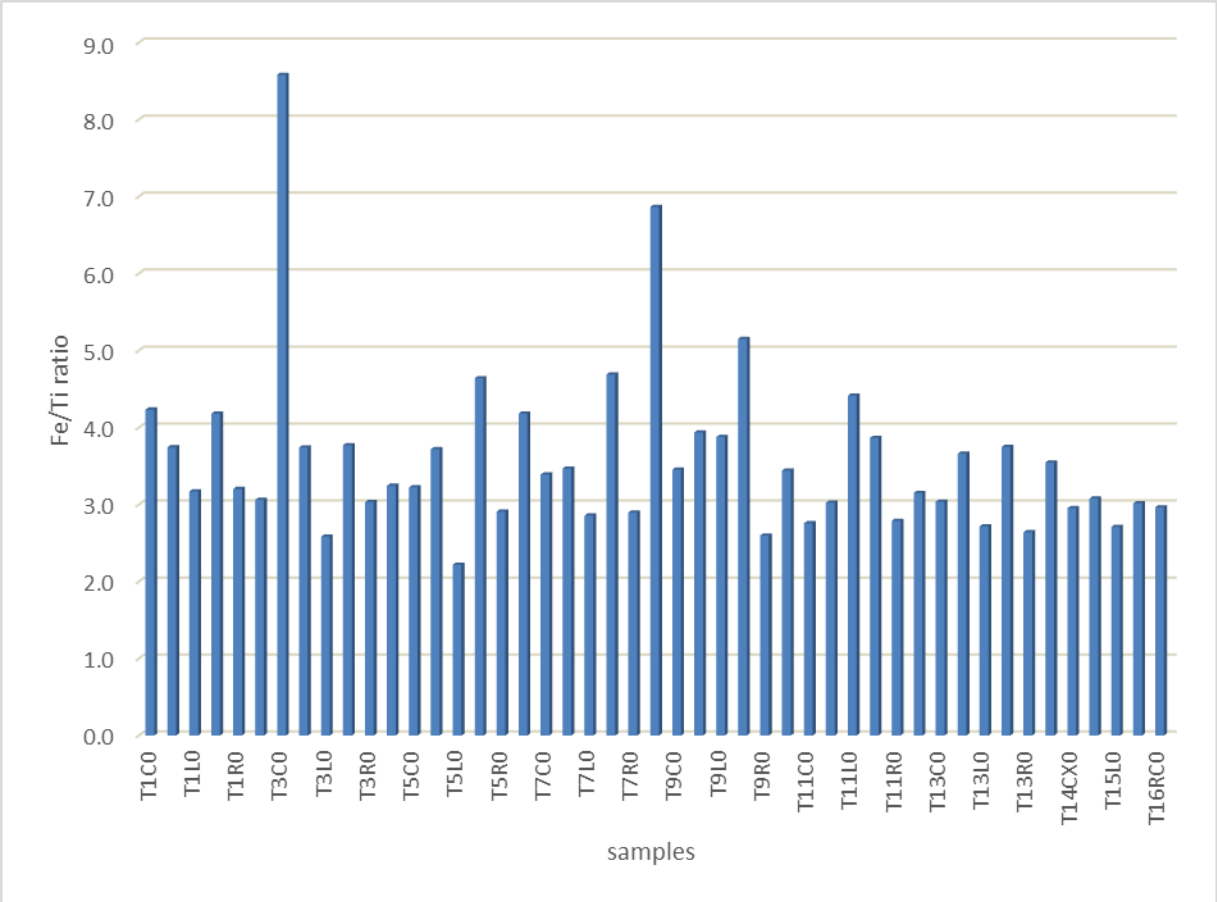

Figure 4.10: Fe/Ti ratios of results of EDXRF analyses

4.9 Principal Component Analysis of EDXRF Results of River Tiva Sands.

In this study, XLSTAT (2015) software was used for PCA based on Pearson linear correlation matrix and the association between calculated components and the original variables, to explore the variation and the interrelationships between different element

concentrations and to detect sample patterns and variable relationships within and between sites (Appendix 9). The results of PCA analysis were used to describe the characteristic geology of the sand, by identifying those components responsible for the mineralogical variability of the deposits (Leinen and Pisias, 1984).

Table 4.7a and Table 4.7b shows that two principal components can explain 80.249% of the elemental variability in river Tiva; PC1 groups Fe, Ti, V, Mn, Zr and accounts for 64.98% of the total variability, PC2 explains Cu and Sr, accounts for 15.27% of the total variability. In this study, we have considered factors with eigenvalues greater than 1 (Chen et al., 2007). Two independent factors that explained samples from Tiva were represented by the first and second principal components that groups Ti, V, Mn, Fe, and Zr and has all elements fairly correlated (loading more than 0.8) and are indicative of the heavy minerals presence in river Tiva sands (Table 4.8).

Table 4.7a: Summary of the results of the principal component analysis

	F1	F2	F3	F4	F5	F6	F7
Eigenvalue	4.549	1.069	0.835	0.372	0.114	0.052	0.009
Variability (%)	64.983	15.266	11.930	5.320	1.624	0.750	0.126
Cumulative %	64.983	80.249	92.180	97.500	99.124	99.874	100.000

Table 4.7b: Contribution of the variables to the principal components

	F1	F2	F3	F4	F5	F6	F7
TI	0.454	-0.005	-0.151	-0.255	-0.235	-0.382	0.710
V	0.445	0.065	-0.066	-0.393	0.122	0.789	0.026
MN	0.445	0.011	-0.037	0.206	0.820	-0.276	-0.095
FE	0.442	-0.205	-0.154	-0.247	-0.359	-0.291	-0.681
CU	-0.061	0.853	-0.496	-0.023	-0.036	-0.079	-0.123
SR	0.193	0.474	0.837	-0.105	-0.093	-0.113	-0.072
ZR	0.401	0.049	-0.023	0.815	-0.344	0.226	0.040

Figure 4.11 shows the scree plot of the variables and it shows that the first principal component which explains the variability of the mineralogy of the sands.

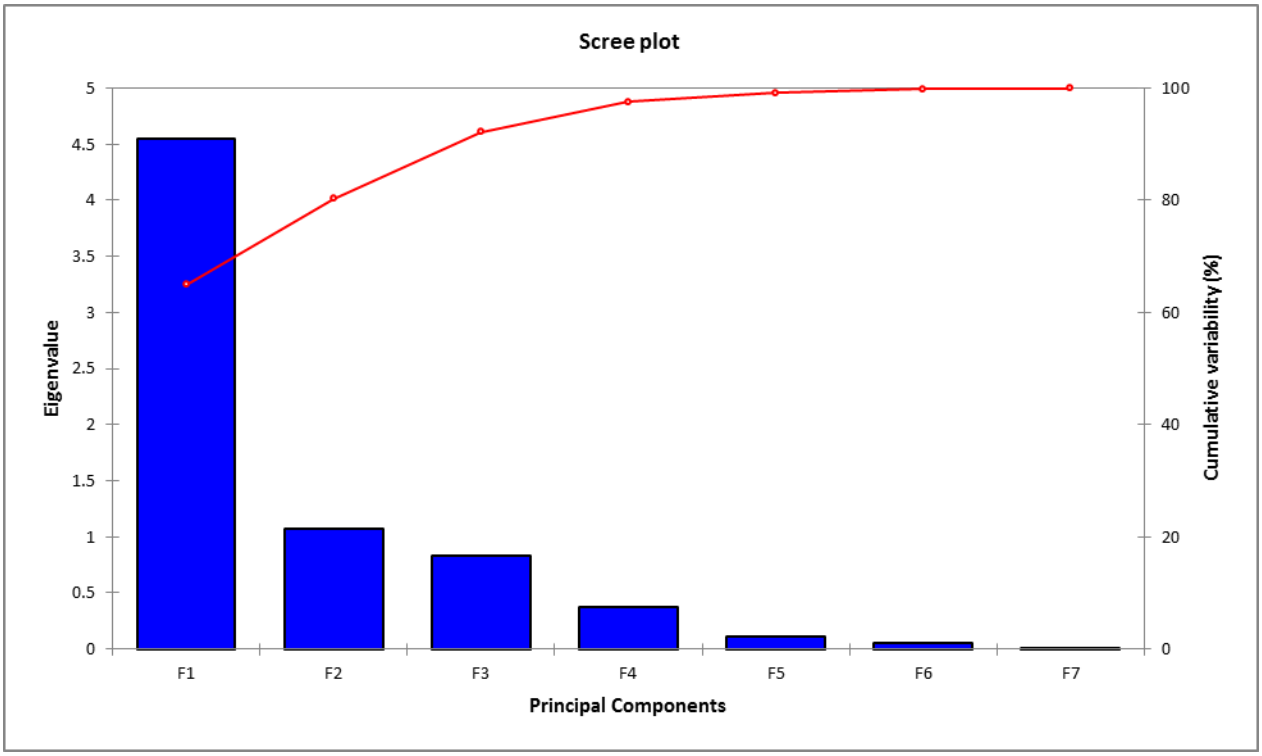

Figure 4.11: Scree plots of the variables, eigenvalues, principal components and cumulative variability

Table 4.8: Shows the factor loading of the Elements contribution in principal components

	F1	F2	F3	F4	F5	F6	F7
Ti	0.969	-0.005	-0.138	-0.156	-0.079	-0.088	0.067
V	0.949	0.067	-0.061	-0.240	0.041	0.181	0.002
Mn	0.950	0.011	-0.034	0.126	0.277	-0.063	-0.009
Fe	0.943	-0.212	-0.141	-0.151	-0.121	-0.067	-0.064
Cu	-0.130	0.881	-0.453	-0.014	-0.012	-0.018	-0.012
Sr	0.411	0.490	0.765	-0.064	-0.031	-0.026	-0.007
Zr	0.856	0.051	-0.021	0.498	-0.116	0.052	0.004

The PCA analysis of the trace elements concentrations of interest indicate pattern of the elements variability relating to the mineralogy of the sands. The sorting of the titanomagnetite heavy mineral (Ti and Fe) is apparent along the F1 axis (Figure 4.12). The first two PCA axes contributed for 80.25 %(F1-64.98% and F2-15.27%) of the total variance within the dataset (Figure 4.12).

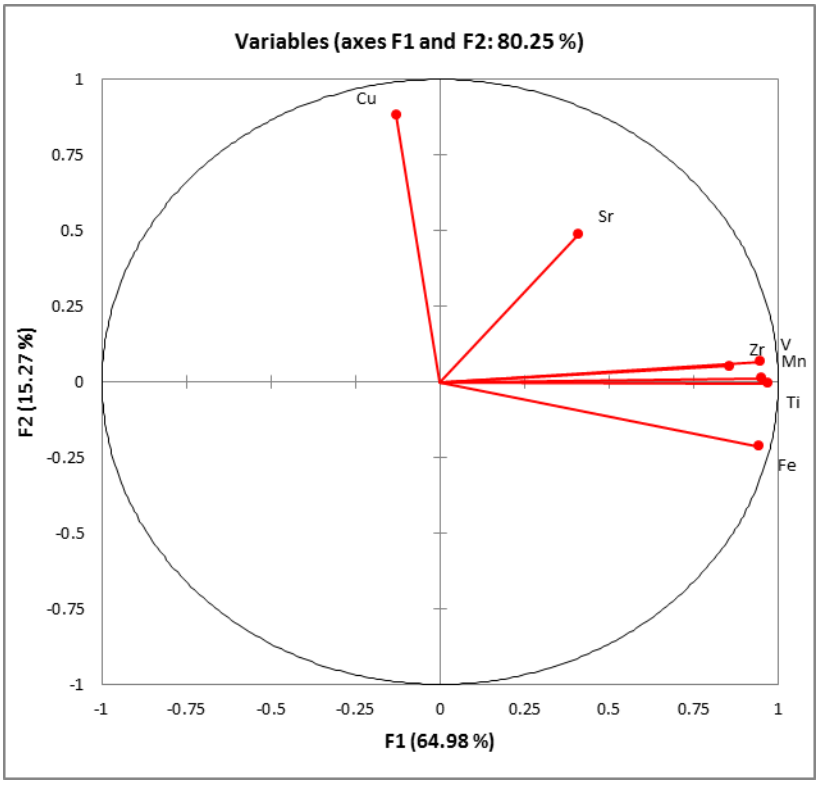

Figure 4.12: Factor loading of the variables

The factor scores plot were used to identify the origin of the heavy minerals in these samples (Osán et al. 2002). The circled locations sampled (figure 4.13) contributed to the first principal component, whereby heavy minerals are a lot more concentrated. These samples are all represented from the Tanganyika area (figure 4.13).

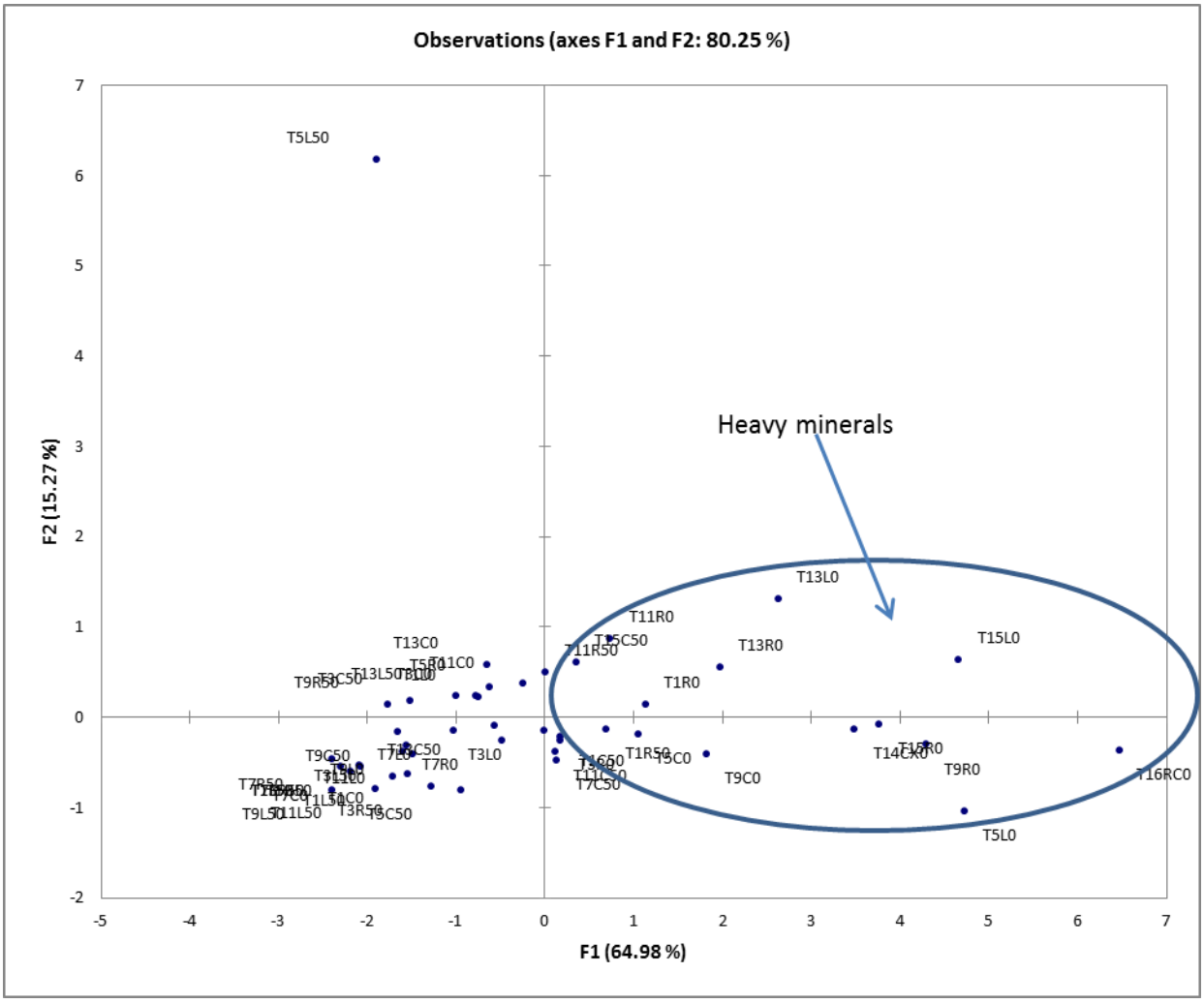

Figure 4.13: Contribution of the sites to F1 and F2

Figure 4.14 shows the biplot of the transformed data for the PC1 and PC2. From which Fe and Ti are grouped together indicative of the similar source of origin of mineralogy. Also, evidenced by the strong correlation between the two elements (Appendix 10). Zirconium is separately located hence slightly contribute to PC2 (Figure 4.12). Zirconium is derived from zircon minerals and therefore not correlated with other elements of interest; Fe and Ti in these samples.

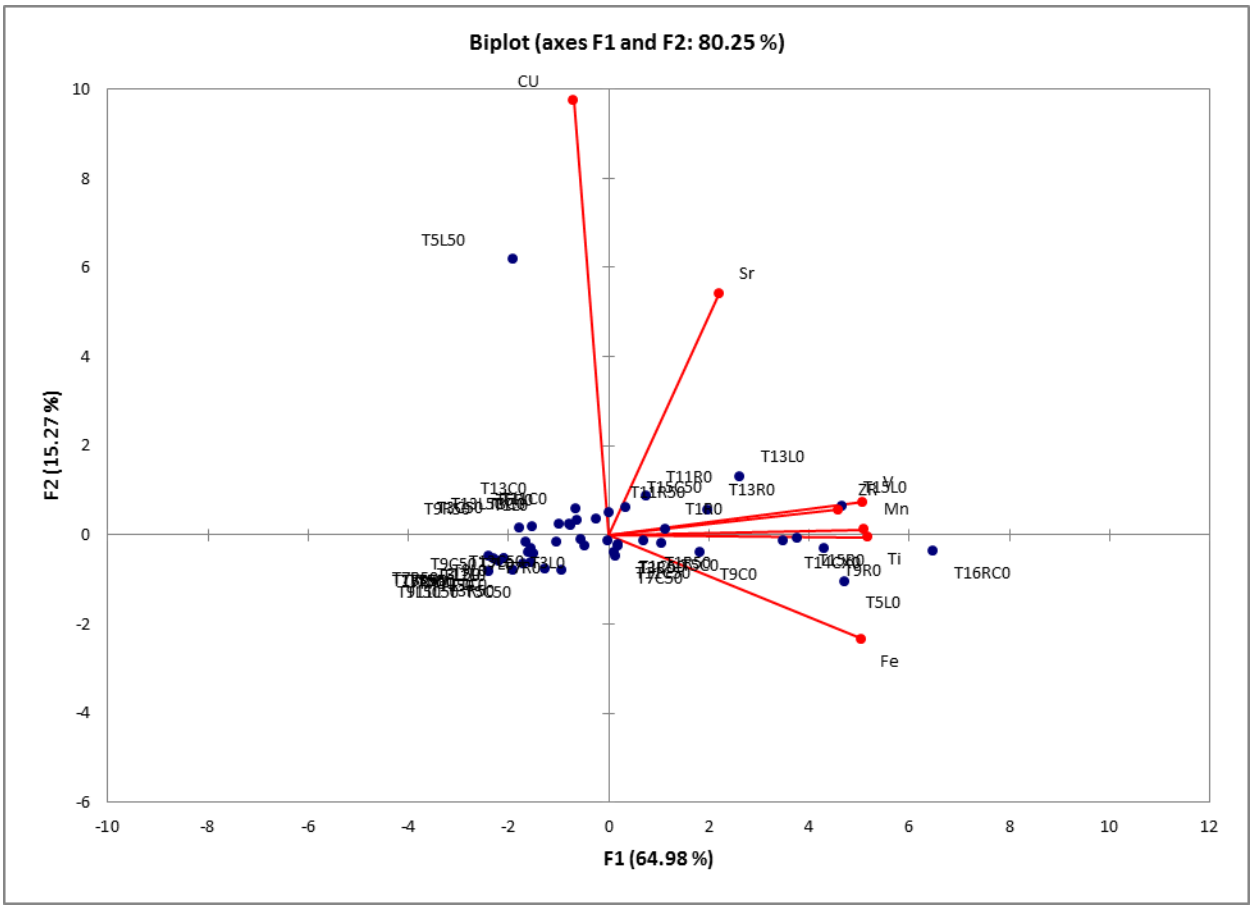

Figure 4.14: Biplot based on the principal component, F1 verses F2.

CHAPTER FIVE

CONCLUSIONS AND RECOMMENDATIONS

5.1 Conclusions

In summary, this study has demonstrated that river Tiva is characterized by large deposits of sands that are magnetic and indicative of heavy minerals. The geology of the study area indicates the presence of the igneous and sedimentary rocks associated with the occurrence of the heavy minerals. Most of these sands are presently harvested for building and construction industry.

The results of EDXRF analyses show that Fe concentration was dominant at 73135±6027µg/g, followed by at Ti 22976±1971µg/g and Zr at 1115±13µg/g. This study has successfully demonstrated the presence of heavy minerals as some of the constituents of river Tiva sands.

The results for river Tiva sands characterization for heavy minerals in this study has been complemented by XRD analyses for mineral composition; ilmenite and hematite. In general, these sands are characterized by high concentration of quartz approximately (40.33%) on average. Other minerals of economic relevance identified include; hematite (7.99%) and ilmenite (4.09%).

In addition, river Tiva black sands are categorized as titanomagnetite following higher values of Fe/Ti ratios that accounts for the high magnetic property. The results of this study are in agreement with other related studies done elsewhere (Temple, 1966). The correlation between Fe and Ti (r=0.9637) is indicative of same source origin. Also, evidenced by principal component analysis of the data, in which PC1 has grouped together Fe and Ti. Zr in the mineral samples is grouped in PC2 and therefore has an origin different from that of Fe and Ti.

In conclusion, most of heavy minerals are more concentrated downstream. In most cases, higher levels of the elements studied, are concentrated at the sub-surfaces (<50cm). There was no statistical significant difference in the distribution of the heavy minerals across

the river bed following ANOVA analyses of data (Zr, p=0.24; Zr, p=0.7; Fe, p=0.7) at 95% confidence level.

The results of this study are significant for further heavy mineral exploration and exploitation in the study area.

5.2 Recommendations

The study, therefore, recommends the following:

1) Heavy mineral separation studies;
2) Provenance studies for the source apportionment of the heavy mineral sands;
3) Other complementary characterization techniques of heavy minerals used; SEM-EDX, optical microscope and grain counting for the analyses of heavy minerals;
4) Studies on interrelationship with river Tiva and Kwale heavy mineral sands; and
5) Mineralogical studies to determine the extent of ilmenite alteration specifically for the presence of leucoxene.

REFERENCES

Abuodha, J. O. Z (2003). Grain size distribution and composition of the modern dune and beach sediments, Malindi Bay Coast, Kenya, *Journal of African Earth Science*, **36(1)**, 41-54.

Addinsoft. (2010). *XLSTAT 2015*, Data analysis and statistics software for Microsoft Excel**.** Retrieved, October 10, 2015, from https://www.xlstat.com/en/.

Anjos, M. J., Lopes, R. T., Jesus, E. F. O., Simabuco, S. M., and Cesareo, R. (2002). Quantitative determination of metals in radish using x-ray fluorescence spectrometry. *X-ray Spectrometry*, **31(2),** 120-123.

Aral, H. and Mcdonald, K. J. (1999). Radioactive impurity removal from zircon sands by heat and leach process. - *In: STIMSON, R.G. (ed.): Heavy Minerals.* - *South African Institute of Mining and Metallurgy, Symposium Series*, S23: 171 - 176, 6 tab., Johannesburg, RSA

Babu, N., Vasumathi, N., and Rao, R. B. (2009). Recovery of ilmenite and other heavy minerals from Teri Sands (red sands) of Tamil Nadu, India. *Journal of Minerals and Materials Characterization and Engineering*, **8(02**), 149.

Base Resources Ltd. (2011). Quarterly activities report—December 2010: West Perth, Western Australia, Australia, *Base Resources Ltd*., 15 p. Retrieved August 4, 2012, from www.baseresources.com.

Berquist Jr, C. R. (2010, March). Recent advances of geologic mapping in the Virginia Coastal Plain. In *Geological Society of America Abstracts with Programs*, (Vol. 42, No. 1, p. 101).

Bertin, E.P. (1975). *Principles and Practice of X-ray Spectrometric Analysis, 2nd ed*. New Jersey: Plenum, p93-160.

Chandrajith, R., Dissanayake, C. B., & Tobschall, H. J. (2001). Application of multi-element relationships in stream sediments to mineral exploration: a case study of Walawe Ganga Basin, Sri Lanka. *Applied Geochemistry*, **16(3),** 339-350.

Chen, K., Jiao, J. J., Huang, J., & Huang, R. (2007). Multivariate statistical evaluation of trace elements in groundwater in a coastal area in Shenzhen, China. *Environmental Pollution*, **147(3**), 771-780.

Clarke, G. (1986). Titanium minerals. Expansions in all the continents. *Ind. Miner*, **(225**), 47.

Cullity, B. D. (1978). *Elements of X-Ray Diffraction*. USA: Edison-Wesley P Inc, p 20-132.

De Meijer, R. J. (1998). Heavy minerals: from Edelstein 'to Einstein. *Journal of Geochemical Exploration*, **62(1),** 81-103.

De Meijer, R.J., Lesscher, H.M.E, Schuiling.R.D, and Elburg. M.E (1990). Estimate of heavy mineral content in the sand and its provenance by radiometric means. *Nuclear Physics*, **4**,455-460.

Dryden, L., & Dryden, C. (1946). Comparative rates of weathering of some common heavy minerals. *Journal of Sedimentary Research*, ***16*(3),**91-96.

Elsner, H. (2010). *Heavy Minerals of Economic Importance, Assessment Manual*. *Retrieved June 15, 2012*, www.bgr.bund.de/DERA/DE/.../Heavy-Minerals-Economic-Importance.pdf?__blob...

Falkenberg, G. (2002). X-ray Fluorescence (XRF), Applications of Synchrotron Radiation in Environmental Science, CAMD Summer School.

Force, E.R. (1991). Geology of titanium mineral deposits. *Geol. Soc*, **259**, 112.

Gajah, D. K. B. L. K. (2009). Determination of Heavy Minerals in 'Amang'from Kampung Gajah Ex-Mining area. *Malaysian Journal of Analytical Sciences*, ***13*(2**), 194-203.

Garnar Jr, T. E. (1984, February). Mineralogical methods used in the heavy mineral industry. In *Applied Mineralogy*. Proceedings of the Second International Congress on Applied Mineralogy in the Minerals Industry, *Metallurgical Society of the AIME*, (pp. 297-312).

Garnar, T.E. JR. (1980). Heavy minerals industry of North America. - Proc. 4th"Industrial Minerals" Internat. Congr. Atlanta: 29 – 42, 13 fig., 4 tab.; Atlanta, GA.

Gent. M.R., M.N. Alvarez, J.M.G Iglesias, and J.T Alvarez. (2005). Offshore occurrences of the heavy-mineral placers, Northwest Galcia, Spain. *Mar, Georesour Geotec*., **23**, 39-59

Gillson, J. L. (1959). Sand deposits of titanium minerals. *Mining Engineering*, ***11***(4), 421-429.

Grosz, A. E., & Schruben, P. G. (1994). NURE geochemical and geophysical surveys; defining prospective terranes for United States placer exploration (No. 2097). USGPO; for sale by US Geological Survey, Information Services, Retrieved February 26, 2014, from http://pubs.usgs.gov/bul/2097/report.pdf

Hamzah, Z., Alias, M., Saat, A., Wood, A. K., & Tajuddin, Z. (2007). Surface radiation dose measurement and mapping of Jengka 15 oil palm land. *Malaysian Journal of Analytical Sciences*, ***11*(1),** 237-245.

Hawkes, H. E. (1957). *Principles of geochemical prospecting* (No. 1000). Arvada,USA: USGPO,p226.

Hill, R. J., & Howard, C. J. (1987). Quantitative phase analysis from neutron powder diffraction data using the Rietveld method. *Journal of Applied Crystallography*, **20(6),** 467-474.

Hollyer, G. M., Minton, T., & Daniels, A. (1999). Integrated Presentation and Interpretation of Geochemical Data and Multi-disciplinary Information: Regional and Local-Scale Approaches. *IGES, Vancouver, Canada_*. Retrieved February 23, 2014, from http://www.geosoft.com.br/media/uploads/resources/success-stories/aa_cs_2008_01_web.pdf

Ige, A., & Rehren, T. (2003). Black sand and ironstone: iron smelting in Modakeke, Ife, and southwestern Nigeria. *Institute for Archaeo-Metallurgical Studies*, ***23***, 15-20.

Jenkins, R., and Gilfrich, J. V. (1992). Figures-of-merit, their philosophy, design, and use. *X-Ray Spectrometry*, **21(6),** 263-269.

Kaminsky, H. A., Etsell, T. H., Ivey, D. G., & Omotoso, O. (2008). Characterization of heavy minerals in the Athabasca oil sands. *Minerals Engineering*, **21(4),** 264-271.

Kariuki, D. (2002). Natural resources - Minerals: A report of the civil society review of the implementation of Agenda 21 in Kenya. *Kenya NGO Earth Summit 2002 Forum*. Retrieved July 23,2012, from http://www.worldsummit2002.org/texts/KENYAminerals.pdf

Kim, W. T., Shin, H. Y., Lee, J. C., Jeon, H. S., Chang, S. W., & Choi, H. S. (2006). Recovery of Heavy Minerals from Korean Beach Sand. n: *Proceedings of the International Seminar on Mineral Processing Technology and Indo-Korean Workshop on Resource Recycling* (MPT-2006), March 8-10, 2006, NML, Chennai. Retrieved June 15, 2014, from http://eprints.nmlindia.org/6299.

Kitui County. (n.d).*Overview of Kitui County*. In Kenya information guide. Retrieved November 25, 2015 from http://www.kenya-information-guide.com/kitui-county.html

Knudsen, C. (2005). Multi-method approach to heavy mineral exploration: Miocene of Denmark. In *2005 Heavy Minerals Conference Proceedings* (p. 83). Society for Mining Metallurgy.

Leinen, M, and Pisias, N. (1984). An objective technique for determining end member compositions and for partitioning sediments according to their sources. *Geochimica et Cosmochimica Acta*, **48**, 47-62.

Lener, E. F. (1997). *Mineral Chemistry of Heavy Minerals in the Old Hickory Deposits*. Sussex and Dinwiddie Counties, Virgenia. M. Sc Thesis, Faculty of the Virginia, Polytechnic Institute, State University.

Li, M. Z. and Komar, P. D. (1992). Longshore grain sorting and beach placer formation adjacent to the Columbia River. *J. Sediment Petrol*., **62(3)**, 429-441.

Li, M. Z., & Komar, P. D. (1992). Selective entrainment and transport of mixed size and density sands: Flume experiments simulating the formation of black-sand placers. *Journal of Sedimentary Research*, 62(4), 584-590.

Lowright, R., Williams, E. G., & Dachille, F. (1972). An analysis of factors controlling deviations in hydraulic equivalence in some modern sands. *Journal of Sedimentary Research*, ***42*(3),** 635-645.

Mangala, M. J., and Patel, J. P. (1996). X-ray fluorescence analysis of fluorite minerals for major and trace constituents. *J. Trace and Microprobe Techniques*, **14(4),** 703-740.

Martin, W. R. B., & Long, A. M. (1960). Heavy mineral content and radioactivity counts of the beach sands west of Oreti river mouth to Blue Cliffs, Southland, New Zealand. *New Zealand journal of geology and geophysics*, ***3*(3**), 400-409.

Mason, B. & Moore, C.B. (1982). *Principles of Geochemistry*. 4th edition, New York, N.Y: John Wiley and Sons, Inc, pp344.

Mathu, E. M., & Tole, M. P. (1984). Geology of the Ithanga Hills in Kenya. *Journal of African Earth Sciences (1983)*, ***2*(1),** 1-16.

Mesfin, W.G., Godfrey, R.L., Nkini, E.C., & Kimaro, L.M. (2006). Mineral potential of SEIMIC member countries.Retrieved April 18, 2016, from www.seamic.org/Vol9_No1.pdf

Misra, N. L., & Mudher, K. S. (2002). Total reflection X-ray fluorescence: a technique for trace element analysis in materials. *Progress in crystal growth and characterization of materials*, ***45*(1),** 65-74.

Mori, P. E., Reeves, S., Correia, C. T., and Haukka, M. (1999): Development of a fused glass disc XRF facility and comparison with the pressed powder pellet technique at instituto de geociencias, Sao Paulo University. *Brazilian Journal of Geology*, **29(3**), 441-446.

Morton, A. C., & Hallsworth, C. (1994). Identifying provenance-specific features of detrital heavy mineral assemblages in sandstones. *Sedimentary Geology*, **90(3)**, 241-256.

Mucke, A. & Chaudhuri, J.N.B. (1991). The continuous alteration of ilmenite through pseudorutile to leucoxene. *Ore Geol. Reviews* ***6***, 25-44.

Munyiri, S. (2009). Policy Position Paper on the Proposed Amendments of the Mining and Minerals Bill 2009. Nairobi: Kenya Chamber of Mines. *Retirieved July 9, 2012,* from *ww.businessadvocacy.org/dloads/ppp%20KCM%20**mining**&**minerals**.pdf*

Nair, A.G., Damodaran, K.T., and Suresh Babu, D.S. (1995). Mineral-Chemical analysis of ilmenites from the River Valliyar and the Manavalakurichi Beach, Tamil Nadu. *J. Geol. Soc. India*, **46**, 655-61.

Nallusamy, B., Babu, S., & Babu, D. S. (2013). Heavy mineral distribution and characterisation of ilmenite of Kayamkulam—thothapally Barrier Island, southwest coast of India. *Journal of the Geological Society of India*, **81(1),** 129-140.

Nyambura, M., Gatari, M., Hillier, S., Shepherd, K. D., Esala, M., & Mochoge, B. (2014). Development of an X-ray method for mineralogical analysis of Africa soils using a benchtop diffractometer. In *Food and nutrition security in Africa: FoodAfrica midterm seminar in Helsinki 16th June 2014: a book of abstracts/Rokka, Susanna (ed.)*. MTT.

Osan, J., Kurunczi, S., Török, S., & Van Grieken, R. (2002). X-Ray analysis of riverbank sediment of the Tisza (Hungary): identification of particles from a mine pollution event. *Spectrochimica Acta Part B: Atomic Spectroscopy*, **57(3),** 413-422.

Pirkle, F. L., & Podmeyer, D. A. (1993). Zircon: origin and uses. *Transactions*, **292**, 1-20.

Potgieter-Vermaak, S. (2007). Surface characterization of a heavy mineral sand with micro-Raman spectrometry. In *6th International Heavy Minerals Conference 'Back to Basics'. The Southern African Institute of Mining and Metallurgy, Johannesburg* (pp. 49-53).

Pourjabbar, A., & Hezarkhani, A. (2006). Heavy Mineral Prospecting: A complementary Method for geochemical exploration; A case study in Sarab, Iran. In *6th International Scientific Conference-SGEM* (Vol. 1, pp. 221-232). SGEM Scientific GeoConference.

Rajamanickam, G. V., Varma, O. P., & Gujar, A. R. (1997). Ilmenite placer deposits in the bays of Jaigad, Ambwah, and Varvada, Maharashtra, India. Geology in South Asia - II. Proceedings of the Second South Asia Geological Congress (GEOSAS II), Colombo, Sri Lanka: January 19-24, 1995, Ed. by: Wijayananda, N.P.; Cooray, P.G.; Mosley, P. 325-336.

Rao, N. S., & Misra, S. (2009). Sources of monazite sand in southern Orissa beach placer, eastern India. *Journal of the Geological Society of India*, **74(3),** 357-362.

Reyneke, L., and Van Der Westhuizen, W. G. (2001). Characterisation of a heavy mineral-bearing sample from India and the relevance of intrinsic mineralogical features to mineral beneficiation. *Minerals Engineering*, **14(12),** 1589-1600.

Rietveld, H. (1969). A profile refinement method for nuclear and magnetic structures. *Journal of Applied Crystallography*, **2(2),** 65-71.

Robb, L. (2005). Introduction to Ore-forming Processes. Oxford, UK: Blackwell Publishing, pp. 230-357.

Rop, B. (2010). *Interactive Discussion on Mining.* At the Interactive Discussion on Mining in the 18th Session of the United Nations Commission on Sustainable Development held in NewYork, USA, p.1-5. Retrieved June 23, 2013, from https://sustainabledevelopment.un.org/content/.../658Kenya.pdf.

Rozendaal, A., Philander, C., and de Meijer, R.J. (1999). Mineralogy of heavy mineral placers along the west coast of South Africa. *Heavy Minerals*, South African Institute of Mining and Metallurgy. pp. 67–73.

Rubey, W.W. (1933). The size distribution of heavy minerals within the water-laid sandstone. *Sed. Petrol*. **3**, 3-29.

Sanders, L. D (1954). Geology of the Kitui Area, geological survey of Kenya, government printer, Nairobi, degree sheet 53 pp. 1-10.

Skoog, D.A. and Leary, J.J. (1992). *Principles of Instrumental Analysis*. 4th Edition. Orlando, Florida: Saunders College Publishing, pp 357-359.

Slingerland, R. & Smith, N. D. (1986). Occurrence and formation of water-laid placers. *Annu. Rev. Earth Planet. Sci*. **14**, 113-147

Slingerland, R.L. (1977). The effects of entrainment on the hydraulic equivalence relationships of light and heavy minerals in sands. *J. Sed. Petrol*. **47**, 753-770.

Subramanyam, N.P., Rao, N.K. Narasimhan, D., Rao, G.V.U., Jaggi, N.K. and Rao, K.R.P.M. (1982). Alteration of beach sand ilmenite from Manavalakurichi, Tamil Nadu, India. *J. Geol. Soc. India*, **23**, 168-74.

Temple, A. K. (1966). Alteration of ilmenite. *Economic Geology*, **61(4)**, 695-714.

Tourtelot, H. A. (1968). Hydraulic equivalence of grains of quartz and heavier minerals, and implications for the study of placers (No. 594-F). *Retrieved December 14, 2014, from https://pubs.er.usgs.gov/publication/pp594F.*

Tyler, R. M., & Minnitt, R. C. A. (2004). A review of sub-Saharan heavy mineral sand deposits: implications for new projects in southern Africa. *Journal-South African Institute of Mining and Metallurgy*, ***104*(2),** 89-100.

TZMI (2001). *Mineral Sands Annual Review*. Retrieved December 8, 2012, from http://www.tzmi.com.

Vanes, H. J., Vainshtein, D. I., De Meijer, R. J., Den Hartog, H. W., Donoghue, J. F., & Rozendaal, A. (2002). Mineral zircon: A novel thermoluminescence geochronometer. *Radiation effects and defects in solids*, ***157*(6-12),** 1063-1070.

Vision, K. 2030 (2007). *A Globally Competitive and Prosperous Kenya*. *Retrieved June 15,2012,* from https://www.opendata.go. Ke/download/jih3-amby/application/pdf.

Volp. K.M, Russill. J, Brodie- Good.B, and O'Donovan. G. (2009). Exploration for offshore heavy mineral sands by Grupo Minero Esmeralda Colombiana, Colombia. The 7th International Heavy Minerals Conference. The South African Institute of Mining and Metallurgy, pp. 163-673.

Waswa, A.K., Nyamai, C.M., Mathu, E., and Ichang'I, D.W. (2015) Application of Magnetic Survey in the Investigation of Iron Ore Deposits and Shear Zone Delineation: Case Study of Mutomo-Ikutha Area, SE Kenya. *International Journal of Geosciences*, **6**, 729-740.

Waswa, O.S., Nyamai, C.M., Mathu, E.M., and Ichang, D.W.(2015). Integration of Geological Mapping and Remote Sensed Studies for the Discovery of Iron-Ore Mineralization in Mutomo-Ikutha Area, SE Kenya. *Universal Journal of Geoscience*, **15(2)**, 39-50.

Webster, J. R., Kight, R. P., Winburn, R. S., and Cool, C. A. (2003). Heavy mineral analysis of sandstones by Rietveld analysis. *Advances in X-ray Analysis*, **46**, 198-203.

APPENDIX 1: GPS Coordinates for Sampling Sites for Mineral Sands along Tiver River

Sample site	Latitude	Longitude	Altitude
T1	-1.3532938	37.87899298	1040
T3	-1.35505392	37.87360668	1035
T5	-1.35983781	37.87383199	1035
T7	-1.35983781	37.87383199	1035
T9	-1.36440285	37.86880779	1032
T11	-1.36805995	37.86899152	1032
T13	-1.37161380	37.87053287	1022
T14	-1.37325522	37.87053287	1020
T15	-1.37347735	37.87241461	1017
T16	-1.37528859	37.87217086	1018

APPENDIX 2: Model used by Berquist (2010) for Elemental Conversion to Oxides for Heavy Minerals (wt.%)

Assay Reconciliation: Modal oxide composition is shown by two different methods, using the elemental compositions from XBSE data

	CF*	1	2	3	4
Ti	0.5995	28.4	29.13	30.15	29.82
Fe	0.699301	29.93	21.41	25.3	24.9
Al	0.5293	0.82	2.36	1.06	1.44
Mn	1.291	1.58	1.38	1.56	1.55
Si	0.4675	2.1	3.77	2.45	2.61
Zr	0.741	3.57	4.73	4.4	4.33

* *Element-to-oxide conversion Factor*

MLA Calc Assay	1	2	3	4	HM QA/QC
TiO2	47.37	48.59	50.29	49.74	**86.24**
Fe2O3	42.80	30.62	36.18	35.61	**9.15**
Al2O3	1.55	4.46	2.00	2.72	**2.35**
MnO	2.04	1.78	2.01	2.00	
SiO2	4.49	8.06	5.24	5.58	
ZrO2	4.82	6.38	5.94	5.84	
Direct Assay (XRF)	**1**	**2**	**3**	**4**	**XRF**
TiO2	45.14	45.68	48.33	47.53	**85.56**
Fe2O3	42.99	30.75	36.49	35.56	**9.72**
Al2O3	2.34	5.24	2.43	3.56	**2.14**
MnO	1.51	1.25	1.47	1.46	
SiO2	5.37	8.97	5.62	6.11	
ZrO2	4.24	6.06	5.48	5.10	

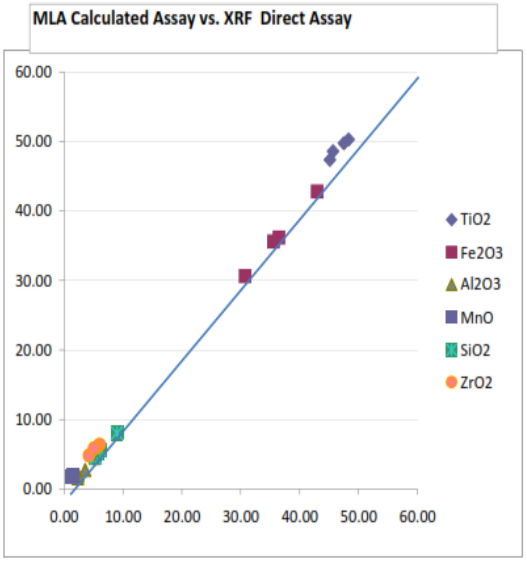

STANDARD QA/QC Rutile Concentrate

Comments:

1 Good reconciliation to direct XRF result indicates accuracy in modal determinations.
2 Slight overstatement of TiO2 is probaby due to inexact mineral chemistry inputs.

APPENDIX 3: Concentration of Ti, Fe and Zr in µg/g for Heavy Mineral Sands from River Tiva

Sample ID	Ti	Fe	Zr
T1C0	12250±1060	47100±3818	504±91
T1C50	25100±1555	94850±5444	899±124
T1L0	19350±2192	58050±7424	546±77
T1L50	11150±353	47100±565	379±42
T1R0	32033±1739	102533±6576	1480±251
T1R50	29850±1909	92000±2969	1605±304
T3C0	17400±2058	50800±5488	503±42
T3C50	10845±1916	41800±3818	423±38
T3L0	24950±2475	83950±9263	991±56
T3L50	11900±1609	44867±5774	399±99
T3R0	25200±1682	76400±5828	920±84
T3R50	18300±794	59333±3288	596±123
T5C0	32700±6155	105400±19028	1430±314
T5C50	19700±1273	69500±4384	787±21
T5L0	55300±4384	170000±12727	4030±495
T5L50	16550±1202	1475±233	686±135
T5R0	15100±141	44150±494	745±70
T5R50	9870±646	41900±2720	379±25
T7C0	10315±544	33800±707	326±51
T7C50	27800±4101	96250±15202	926±190
T7L0	18533±227	54533±4760	679±108
T7L50	7320±321	33367±802	356±26
T7R0	22067±723	63333±3635	1553±302
T7R50	6217±784	27733±4460	277±75
T9C0	34367±3099	118667±9237	1227±25
T9C50	10407±710	40933±4234	454±59
T9L0	12150±1627	47000±3677	320±56
T9L50	6537±717	33667±4479	220±42
T9R0	48033±1305	170000±5568	4427±285
T9R50	9273±863	31900±1609	543±59
T11C0	19233±1222	53000±3610	1220±95
T11C50	24533±1401	74200±3799	1072±133
T11L0	11300±990	43800±6364	374±60
T11L50	12700±458	49067±1986	409±43
T11R0	25150±778	70100±3536	1955±262
T11R50	20333±2593	64033±5777	847±72
T13C0	15750±636	46250±3182	760±161
T13C50	19067±2710	69767±8479	699±106
T13L0	31500±707	85900±3253	2805±346
T13L50	11100±728	41800±2710	707±46
T13R0	34267±737	90467±2854	2047±266
T13R50	11300±953	40067±3092	438±95
T14CX0	59200±3860	181000±1170	687±85
T15C50	21650±1768	65500±7	924±97
T15L0	49367±1665	133667±4619	3377±215
T15R0	40200±2610	131000±8490	3280±213
T16RC0	72667±1862	215333±46918	2210±428
average	**22976±1971**	**73135±6027**	**1115±136**
Min	**62167±784**	**1475±233**	**220±42**
Max	**72667±1862**	**215333±46918**	**4427±428**
	n=3; µ=±1δ		

APPENDIX 4: Results of Oxides in wt. (%) Calculated using Berquist 2010 Model

Sample	TiO_2	Fe_2O_3	ZrO_2
T1C0	2.04	6.74	0.068
T1C50	4.19	13.56	0.121
T1L0	3.23	8.30	0.074
T1L50	1.86	6.74	0.051
T1R0	5.34	14.66	0.200
T1R50	4.98	13.16	0.217
T3C0	2.90	7.26	0.068
T3C50	1.81	5.98	0.057
T3L0	4.16	12.00	0.134
T3L50	1.98	6.42	0.054
T3R0	4.20	10.93	0.124
T3R50	3.05	8.48	0.080
T5C0	5.45	15.07	0.193
T5C50	3.29	9.94	0.106
T5L0	9.22	24.31	0.544
T5L50	2.76	0.21	0.093
T5R0	2.52	6.31	0.101
T5R50	1.65	5.99	0.051
T7C0	1.72	4.83	0.044
T7C50	4.64	13.76	0.125
T7L0	3.09	7.80	0.092
T7L50	1.22	4.77	0.048
T7R0	3.68	9.06	0.210
T7R50	1.04	3.97	0.037
T9C0	5.73	16.97	0.166
T9C50	1.74	5.85	0.061
T9L0	2.03	6.72	0.043
T9L50	1.09	4.81	0.030
T9R0	8.01	24.31	0.597
T9R50	1.55	4.56	0.073
T11C0	3.21	7.58	0.165
T11C50	4.09	10.61	0.145
T11L0	1.88	6.26	0.050
T11L50	2.12	7.02	0.055
T11R0	4.20	10.02	0.264
T11R50	3.39	9.16	0.114
T13C0	2.63	6.61	0.103
T13C50	3.18	9.98	0.094
T13L0	5.25	12.28	0.379
T13L50	1.85	5.98	0.095
T13R0	5.72	12.94	0.276
T13R50	1.88	5.73	0.059
T14CX0	9.87	25.88	0.093
T15C50	3.61	9.37	0.125
T15L0	8.23	19.11	0.456
T15R0	6.71	18.73	0.443
T16RC0	12.12	30.79	0.298
MEAN	**3.83**	**10.46**	**0.151**
MIN	**1.04**	**0.21**	**0.030**
MAX	**12.12**	**30.79**	**0.597**

APPENDIX 5: XRD Results of the River Tiva Sand (wt. %)

sample	Albite	Diopside	Hematite	Hornblende	Ilmenite	Microcline	Orthoclase	Quartz	Tremolite
T8C0	25.1	9.5	10	15.5	6.4	0	0	33.6	0
T10C50	26.6	0	6.2	14.4	0	0	17.2	35.6	0
T10C0	25.6	0	3.2	10.3	0	0	13.7	47.1	0
T12C0	24.7	0	4.2	8.3	0	0	11.6	51.1	0
T14BCX0	28	0	17.3	0	13.4	0	0	29.4	11.9
T14C50	23.3	0	2.1	7.3	0	0	10.1	57.2	0
T14C0	24.2	0	2.2	7.9	0	0	13.4	52.3	0
T14C0	25.6	0	3.9	11.3	0	0	13.5	45.6	0
T16C0	16.4	0	17.8	0	11.5	19.8	0	24	10.6
T16C50	18.3	0	13	0	9.6	22.1	0	27.4	9.7

APPENDIX 6: Results of Distribution and Profiling of Zirconium in µg/g

Sites	Depths	Sampled Positions across the River Bed		
		Left	Centre	right
T1	0cm	545.50	504.00	1480.00
	50cm	379.00	899.00	1605.00
T3	0cm	990.50	503.00	919.67
	50cm	398.67	423.00	595.67
T5	0cm	4030.00	1430.00	745.00
	50cm	685.50	786.50	379.00
T7	0cm	679.00	325.50	1553.33
	50cm	356.00	925.50	276.67
T9	0cm	320.00	1226.67	4426.67
	50cm	220.33	454.00	543.33
T11	0cm	374.00	1220.00	1955.00
	50cm	409.00	454.00	847.00
T13	0cm	2805.00	760.00	2805.00
	50cm	409.00	698.67	707.00
T15	0cm	3376.67	923.50	3280.00
T14	0cm	687.00	687.00	ns
T16	0cm	2210.00	ns	ns

Key:

ns- Not sampled

APPENDIX 7: Distribution and Profiling of Titanium in River Tiva Sand (µg/g)

Sites	Depths	Sampled Positions across the River Bed		
		Left	Centre	Right
T1	0cm	19350	12250	32033
	50cm	11150	25100	29850
T3	0cm	24950	17400	25200
	50cm	11900	10845	18300
T5	0cm	55300	32700	15100
	50cm	16550	19700	9870
T7	0cm	18533	10315	22067
	50cm	7320	27800	6217
T9	0cm	12150	34367	48033
	50cm	6537	10407	9273
T11	0cm	11300	19233	25150
	50cm	12700	10407	20333
T13	0cm	31500	15750	31500
	50cm	12700	19067	11100
T15	0cm	49367	21650	40200
T14	0cm	59200	59200	ns
T16	0cm	72667	ns	ns

Key:

ns- Not sampled

APPENDIX 8: Distribution and Profiling of Iron in River Tiva Sand Samples (µg/g)

Sites	Depths	Sampled Positions across the River Bed		
		Left	Centre	Right
T1	0cm	58050	47100	102533
	50cm	47100	94850	92000
T3	0cm	83950	50800	76400
	50cm	44867	41800	59333
T5	0cm	170000	105400	44150
	50cm	1475	69500	41900
T7	0cm	54533	33800	63333
	50cm	33367	96250	27733
T9	0cm	47000	118667	170000
	50cm	33667	40933	31900
T11	0cm	43800	53000	70100
	50cm	49067	40933	64033
T13	0cm	85900	46250	85900
	50cm	49067	69767	41800
T15	0cm	133667	65500	131000
T14	0cm	181000	181000	ns
T16	0cm	215333	ns	ns

Key:

ns- Not sampled

APPENDIX 9: EDXRF Results of the Sampled Sites (n=3, μ±1δ)

Sample ID	Ti	V	Mn	Fe	Cu	Zn	Sr	Zr
T1C0	12250±1060	841±49	607±30	47100±3818	46±13	53±1	538±69	504±91
T1C50	25100±1555	1450±311	842±104	94850±5444	69±6	99±20	676±82	899±124
T1L0	19350±2192	964±36	649±50	58050±7424	59±5	66±13	751±108	546±77
T1L50	11150±353	814±33	522±61	47100±565	46±5	68±3	535±28	379±42
T1R0	32033±1739	1723±215	1070±98	102533±6576	76±28	98±18	757±63	1480±251
T1R50	29850±1909	1540±141	916±22	92000±2969	86±10	87±22	683±78	1605±304
T3C0	17400±2058	1130±136	723±65	50800±5488	44±3	66±11	746±86	503±42
T3C50	10845±1916	664±181	493±14	41800±3818	45±4	53±24	729±91	423±38
T3L0	24950±2475	1380±57	722±164	83950±9263	75±3	70±14	681±73	991±56
T3L50	11900±1609	603±132	647±280	44867±5774	60±6	51±16	599±84	399±99
T3R0	25200±1682	1478±342	1133±517	76400±5828	54±12	85±10	645±117	920±84
T3R50	18300±794	865±80	527±61	59333±3288	48±5	59±6	518±57	596±123
T5C0	32700±6155	1857±337	1002±282	105400±19028	85±16	118±33	681±16	1430±314
T5C50	19700±1273	966±33	613±88	69500±4384	78±12	63±26	516±16	787±21
T5L0	55300±4384	2324±237	2820±113	170000±12727	65514±4194	191±20	507±27	4030±495
T5L50	16550±1202	1123±239	511±15	1475±233	75400±3960	100±13	696±55	686±135
T5R0	15100±141	995±64	1040±14	44150±494	39±2	75±7	758±13	745±70
T5R50	9870±646	309±61	393±32	41900±2720	44±4	45±5	563±37	379±25
T7C0	10315±544	314±44	424±9	33800±707	40±1	36±12	540±28	326±51
T7C50	27800±4101	1420±14	792±88	96250±15202	79±14	101±16	616±87	926±190
T7L0	18533±227	788±54	593±64	54533±4760	64±14	56±11	659±35	679±108
T7L50	7320±321	350±151	322±32	33367±802	49±2	42±2	553±15	356±26
T7R0	22067±723	874±189	600±110	63333±3635	54±5	60±6	632±105	1553±302
T7R50	6217±784	378±78	311±79	27733±4460	39±2	41±5	565±64	277±75
T9C0	34367±3099	2690±301	1520±56	118667±9237	82±14	133±30	632±37	1227±25
T9C50	10407±710	643±103	521±34	40933±4234	41±3	49±7	648±18	454±59
T9L0	12150±1627	765±45	566±93	47000±3677	45±1	69±3	616±93	320±56
T9L50	6537±717	480±61	370±70	33667±4479	44±6	38±3	490±49	220±42
T9R0	48033±1305	2816±5	1650±125	170000±5568	116±8	161±23	672±21	4427±285
T9R50	9273±863	503±26	417±43	31900±1609	40±7	52±4	712±33	543±59
T11C0	19233±1222	1333±58	773±60	53000±3610	40±3	69±20	767±20	1220±95
T11C50	24533±1401	1800±130	924±39	74200±3799	55±14	88±15	606±90	1072±133
T11L0	11300±990	982±293	639±112	43800±6364	39±4	62±3	586±68	374±60
T11L50	12700±458	531±23	378±49	49067±1986	53±2	47±12	508±37	409±43
T11R0	25150±778	1655±657	733±105	70100±3536	78±2	71±19	892±135	1955±262
T11R50	20333±2593	1487±261	929±68	64033±5777	65±10	77±9	811±50	847±72
T13C0	15750±636	1190±141	675±4	46250±3182	56±1	60±5	819±97	760±161
T13C50	19067±2710	1174±317	691±237	69767±8479	56±3	66±14	683±122	699±106
T13L0	31500±707	2245±290	1745±7	85900±3253	69±30	119±4	993±81	2805±346
T13L50	11100±728	826±83	903±6	41800±2710	44±5	64±7	736±48	707±46
T13R0	34267±737	1953±310	1643±533	90467±2854	70±11	112±11	832±65	2047±266
T13R50	11300±953	158±27	389±7	40067±3092	47±5	39±6	564±57	438±95
T14CX0	59200±3860	3270±356	1510±128	181000±1170	131±15	168±24	766±54	687±85
T15C50	21650±1768	1370±367	1275±49	65500±7	53±14	94±5	840±16	924±97
T15L0	49367±1665	3330±121	2420±95	133667±4619	77±1	157±34	859±54	3377±215
T15R0	40200±2610	3110±236	2210±149	131000±8490	71±8	170±14	690±46	3280±213
T16RC0	72667±1862	5490±1505	2503±603	215333±46918	104±5	234±32	692±157	2210±428
average	**22976±1971**	**1382±268**	**928±111**	**73135±6027**	**3057±181**	**84±13**	**671±61**	**1115±136**
Min	**62167±784**	**157**	**311**	**1475**	**38**	**35**	**489**	**220**
Max	**72667±1862**	**5490**	**2820**	**215333**	**75400**	**234**	**993**	**4427**

APPENDIX 10: Correlation Matrix (Pearson)

Variables	Ti	V	Mn	Fe	Cu	Sr	Zr
TI	**1**	0.945	0.888	**0.969**	-0.064	0.305	0.759
V	0.945	**1**	0.874	0.908	-0.037	0.386	0.702
MN	0.888	0.874	**1**	0.850	-0.102	0.355	0.842
FE	0.969	0.908	0.850	**1**	-0.240	0.192	0.735
CU	-0.064	-0.037	-0.102	-0.240	**1**	0.033	-0.063
SR	0.305	0.386	0.355	0.192	0.033	**1**	0.332
ZR	0.759	0.702	0.842	0.735	-0.063	0.332	**1**